Dynamics of Atmospheres and Oceans 52 (2011) 131–169

Contents lists available at ScienceDirect

Dynamics of Atmospheres and Oceans

journal homepage: www.elsevier.com/locate/dynatmoce

# The California Current System: A multiscale overview and the development of a feature-oriented regional modeling system (FORMS)

Avijit Gangopadhyay[a,*], Pierre F.J. Lermusiaux[b], Leslie Rosenfeld[c], Allan R. Robinson[d], Leandro Calado[e], Hyun Sook Kim[f], Wayne G. Leslie[b], Patrick J. Haley Jr.[b]

[a] *School for Marine Science and Technology, University of Massachusetts at Dartmouth, Suite 325, 200 Mill Road, Fairhaven, MA 02719, United States*
[b] *Department of Mechanical Engineering, Massachusetts Institute of Technology, Cambridge, MA, United States*
[c] *Naval Postgraduate School, Monterey, CA, United States*
[d] *Division of Applied Sciences, Harvard University, Cambridge, MA, United States*
[e] *Marinha do Brasil, Instituto de Estudos do Mar Almirante Paulo Moreira-IEAPM, Rua Kioto, 253-Praia dos Anjos, Arraial do Cabo, RJ 28930-000, Brazil*
[f] *National Centers for Environmental Prediction (NCEP), Silver Springs, MD, United States*

ARTICLE INFO

Available online 19 May 2011

*Keywords:*
California Current System
Feature models
FORMS
Upwelling
Data assimilation

ABSTRACT

Over the past decade, the feature-oriented regional modeling methodology has been developed and applied in several ocean domains, including the western North Atlantic and tropical North Atlantic. This methodology is model-independent and can be utilized with or without satellite and/or *in situ* observations. Here we develop new feature-oriented models for the eastern North Pacific from 36° to 48°N – essentially, most of the regional eastern boundary current. This is the first time feature-modeling has been applied to a complex eastern boundary current system. As a prerequisite to feature modeling, prevalent features that comprise the multiscale and complex circulation in the California Current system (CCS) are first overviewed. This description is based on contemporary understanding of the features and their dominant space and time scales of variability. A synergistic configuration of circulation features interacting with one another on multiple and sometimes overlapping space and time scales as a meander-eddy-upwelling system is presented. The second step is to define the feature-oriented regional modeling system (FORMS). The major multiscale circulation

* Corresponding author. Tel.: +1 508 910 6330; fax: +1 508 910 6374.
*E-mail address:* Avijit@umassd.edu (A. Gangopadhyay).

0377-0265/$ – see front matter 
doi:10.1016/j.dynatmoce.2011.04.003

features include the mean flow and southeastward meandering jet(s) of the California Current (CC), the poleward flowing California Undercurrent (CUC), and six upwelling regions along the coastline. Next, the typical synoptic width, location, vertical extent, and core characteristics of these features and their dominant scales of variability are identified from past observational, theoretical and modeling studies. The parameterized features are then melded with the climatology, *in situ* and remotely sensed data, as available.
The methodology is exemplified here for initialization of primitive-equation models. Dynamical simulations are run as nowcasts and short-term (4–6 weeks) forecasts using these feature models (FM) as initial fields and the Princeton Ocean Model (POM) for dynamics. The set of simulations over a 40-day period illustrate the applicability of FORMS to a transient eastern boundary current region such as the CCS. Comparisons are made with simulations initialized from climatology only. The FORMS approach increases skill in several factors, including the: (i) maintenance of the low-salinity pool in the core of the CC; (ii) representation of eddy activity inshore of the coastal transition zone; (iii) realistic eddy kinetic energy evolution; (iv) subsurface (intermediate depth) mesoscale feature evolution; and (v) deep poleward flow evolution.


## 1. Introduction

The California Current System (CCS) is at the eastern boundary of the wind-driven subtropical gyre in the North Pacific. The region of interest for this system is from 36°N to 48°N and from the North American west coast to 145°W. The dynamics occur on multiple scales in time and space; for example, large-scale gyres and mean southeastward flow are prevalent in climatological averages, while mesoscale eddies and submesoscale filaments are abundant in the synoptic state and are transient in nature. The word "synoptic" is used in this paper to indicate an instantaneous or short-term snapshot of the entire circulation field. Since decorrelation scales in the CCS can be as short as 2 days (Abbott and Zion, 1987; Ramp et al., 2005), currents, eddies, fronts, and filaments that are identifiable in a two-day composite SST or chlorophyll image are considered synoptic. The synoptic state is here generally characterized by interacting free currents and vortices embedded in a background circulation. Synoptic structures are then quite different from a "mean climatological circulation." The mean and synoptic states of a regional ocean can be characterized by a linked set of multi-scale features (Gangopadhyay et al., 1997).

The regional ecosystem is well known for its relatively high productivity and the seasonal and interannual variability resulting from large-scale wind-driven upwelling around its multiple capes and from the irregular occurrences of the El Niño–La Niña phenomenon (Miller, 1996; Miller et al., 2000; Di Lorenzo et al., 2005; Moore et al., 2009). The typical summer circulation is drastically different from that in the winter, and a synoptic description at any one time has been a challenge.

This region has been studied systematically from the early 1950s by the CALCOFI (California Cooperative Oceanic Fisheries Investigation; Wyllie, 1966) monitoring program. However, as in many other regions, the richness of mesoscale variability was recognized first in satellite SST images, and then in color images now available from MODIS and other satellite sensors. The features, their appearance, and prevalent scales available from a synoptic SST image differ from those of a typical climatology (Fig. 1). Clearly, the averaging of data at larger scales masks many of the important mesoscale and submesoscale features.

This region of interest – i.e., the western coast of the U.S. – includes both a larger-scale dynamic offshore region and a finer-scale dynamic coastal region. In recent decades the circulation of the CCS has been studied by observations (Brink et al., 1991; Rosenfeld et al., 1994; Swenson and Niiler, 1996; Ramp et al., 1997a,b; Barth et al., 2000, 2005; Barth and Checkley, 2009). The offshore region is

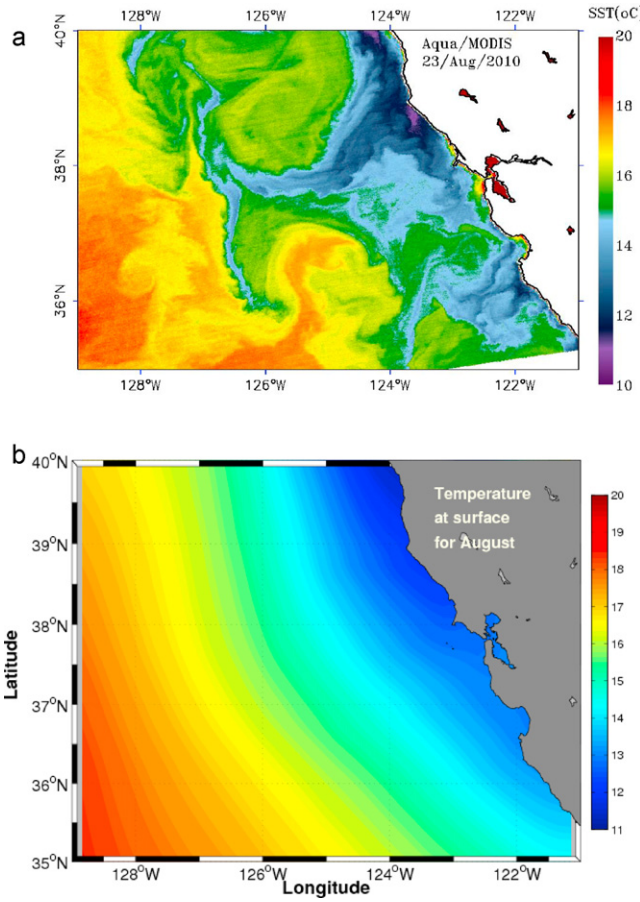


**Fig. 1.** (a) A typical synoptic SST field for the California Current System shows the complex multiscale phenomena along this eastern boundary current region. (b) A typical climatological SST field for August (from Levitus).

primarily dominated by the large-scale California Current and parts of the subtropical and sub-polar gyre circulations in the eastern Pacific. The coastal region includes features such as the California Undercurrent off the continental shelf-break, the upwelling fronts, cold pools inshore of these fronts, jets (narrow high-speed flows), squirts (localized energetic off-shelf flows) (Davis, 1985), mushroom-head vortices, mesoscale and sub-mesoscale eddies, and meanders.

Recent advances in regional modeling and data assimilation have greatly improved our understanding of the complex circulation dynamics in the CCS. Several groups have already demonstrated that it is possible to generate highly realistic simulations of the CCS using long spin-up runs (about 4 years long) (Gruber et al., 2006; Veneziani et al., 2009a) and aggressive data assimilation (Broquet et al., 2009). Some of the noteworthy efforts are: the U.S. Navy's coastal ocean model (Shulman et al., 2007, 2009), UCLA-ROMS (Marchesiello et al., 2003; Gruber et al., 2006; Capet et al., 2008a,b,c), JPL-ROMS (Li et al., 2008a,b), and the UCSC-ROMS Group (Veneziani et al., 2009a,b; Broquet et al., 2009; Goebel et al., 2010).

One of the approaches for regional modeling of such regions in the world oceans is the use of "knowledge-based feature models." This approach is distinctly different from using models to develop the inertia fields in a so-called "spin-up" period, which could be anywhere from one to ten years. Our goal is to develop a feature-modeling system for short-term synoptic forecasting for use where we cannot afford to run models for a long period of time for spin-up or to avoid the build-up of

irreducible model biases, which can occur when numerical codes are run for long periods starting from unrealistic ocean fields. This feature-oriented approach has been used for regional simulations and research-operational forecasting for the past two decades. It originated and was very successful in weather prediction when sufficient data were not available for a complete initialization of features (e.g., Bennett, 1992, chapter 3).

In the ocean, specific examples where feature models (FMs) have been utilized include the studies by Robinson et al. (1989), Hulburt et al. (1990), Hurlburt et al. (1996), Fox et al. (1992), Glenn and Robinson (1995) for Gulf Stream meander and rings (GSMR); Cummings et al. (1997) for the global ocean; Gangopadhyay et al. (1997) for GSMR, Deep Western Boundary Current, and the recirculations in the western North Atlantic; Lermusiaux (1999a) for shelfbreak fronts; and Robinson and Glenn (1999) for adaptive sampling. These authors have applied the FM technique for use in nowcasting, forecasting and assimilation studies using various *in situ* (XBT, CTD), satellite (SST, SSH [GEOSAT, TOPEX/Poseidon], and sea surface color [SeaWiFS]) observations. FMs for naval application have been implemented operationally by the Royal Navy (Heathershaw and Foreman, 1996) and have been developed for global application in a coupled ocean–atmosphere climate prediction mode (Johns et al., 1997).

Gangopadhyay and Robinson (2002) have generalized the feature-oriented approach for application to any regional ocean. A feature-oriented regional modeling system (FORMS) for the Gulf of Maine and Georges Bank region has been developed for real-time applications for medium-range (7–10 days) and mesoscale to sub-mesoscale forecasting (Gangopadhyay et al., 2003; Brown et al., 2007a,b). This feature-oriented methodology is also model-independent and can be applied in lieu of either satellite or *in situ* observations, or both, especially in coastal regions. It has been used in many real-time simulations, including the recent Cyber Infrastructure component of the Ocean Observatory Initiative efforts (Schofield et al., 2010).

The purposes for developing FORMS in any region are many. The most important ones include: (i) providing multiscale initial field to a 3D dynamical model for nowcasting and short-term forecasting; (ii) understanding processes and dynamical interactions between features and forcing by carrying out sensitivity studies with and without features in a 4D numerical experiment; (iii) assimilating pre-existing dynamical FMs in lieu of, or in addition to, satellite or *in situ* observations in a 4DVAR-like assimilation. FMs are also useful for biogeochemical process studies (Hasegawa et al., 2009), for acoustic propagation through eddies (Carriere et al., 2010), and in ensemble forecasting for an Observation System Simulation Experiment (Schofield et al., 2010). They are also being used for routine forecasting in the western North Atlantic (Schmidt and Gangopadhyay, under review) and for the Trinidad-North Brazil Current Ring region (Schmidt et al., 2011).

The objective of this manuscript is to develop a set of FM for the California Current System. This is the first extension of the FM framework to any eastern boundary upwelling ecosystem. The developed FMs are used to initialize a POM model run (FM-POM). The skill of the FM-POM run is evaluated by comparing with the POM model initialized with Levitus climatology (Levitus-POM). The results show that FM-POM generates mesoscale features such as surface and subsurface eddies, upwelling filaments and jets, eddies off of the CUC, and maintains the low salinity pool along the CC. Furthermore, when compared to Levitus-POM, FM-POM generates more energetic mesoscale features in both surface and subsurface layers.

For synoptic forecasting, it is necessary to resolve dynamic evolution of meanders, cross-frontal exchanges, eddy-frontal interactions, upwelling-jet-filament evolution, etc. A set of strategic locations based on such dynamical considerations for all of the features is called the "multiscale synoptic circulation template" for the region. In other words, this basis template is the regional map of dynamically strategic locations for placing FM profiles. These profiles provide "synthetic synoptic expressions" for fronts, jets, eddies, gyres, and other circulation structures and water masses at the initialization or updating phases. Features are represented both by analytical structures and by synoptic sections and profiles of temperature and salinity. The FM profiles for a typical feature are developed by analyzing past synoptic high-resolution observations for that feature. The generalized mathematical forms for some of the typical FMs developed so far have been described by Gangopadhyay and Robinson (2002, see their Appendix A). A number of applications for coastal regions such as a coastal current, tidal mixing front, eddies and gyres have also been described (Gangopadhyay et al., 2003).

For an oceanic region such as the CCS, such structures and parameterized forms can be implemented to characterize the relevant circulation entities. Such implementation requires careful and detailed scientific analyses to identify the variability that define and distinguish these features from one another while preserving the particular characteristics and dynamic balances of each feature. After major features are identified and individually represented, they are used in the initialization of a dynamical model (e.g., POM). Dynamical adjustment accomplishes two important tasks: (i) a consistent dynamical interaction of the features, and (ii) the generation of smaller-scale features, such as squirts and sub-mesoscale eddies.

This study builds on the experience and knowledge from the above studies to develop FORMS for the CCS. The application of FORMS for nowcasting and forecasting is of interest to the US Navy, CeNCOOS (Central California Coastal Ocean Observation System), SCCOOS (Southern California Coastal Ocean Observation System) and similar entities. Section 2 provides a multiscale overview of the CCS circulation. Section 3 presents a synopsis of the CCS features and their variability, which is the prerequisite first step from a feature-oriented regional modeling perspective. The individual FMs are described in Section 4. The FORMS protocol for initialization for this region is then illustrated in Section 5. Dynamical simulations using climatology and selected FMs are discussed in Section 6. Section 7 summarizes the results, and also outlines the future directions for maintaining longer-term feature-oriented regional forecasts.

## 2. A brief overview of the multiscale nature of the CCS

The instantaneous California Current (CC) was first described by Mooers and Robinson (1984) as an energetic meandering jet, interacting with mesoscale eddies and coastal upwelling regions. During the OPTOMA (Ocean Prediction through Observation, Modeling and Analysis) exercises in the summers of 1983 and 1984, Robinson et al. (1984, 1986) designed the first real-time dynamical forecasting experiment in the CCS region and found that the time-scales of eddy-meander/eddy-eddy interactions are on the order of 1–2 weeks there.

A coastal transition zone (CTZ) along the California coast was first defined by Brink et al. (1991) as the demarcation between the faster, more energetic, shallow and narrow coastal upwelling-dominated flow system and the large-scale, broad mean southward flow in the deep offshore region. The transition zone was thought to be an area where mesoscale eddies and filaments would dominate. The CC core was proposed by Strub et al. (1991) as a strong surface jet meandering through a field of associated cyclonic and anticyclonic eddies. They also found evidence of some subsurface eddies which had no identifiable surface signatures. An end-of-the-century overview of the CCS, its seasonality and interannual variability was provided by Hickey (1998), who also identified the core of the current as a freshwater signature, different from the coastal upwelling water masses.

A compilation of the physical, chemical and biological studies of the CCS over the past century was organized by Chavez and Collins (2000a,b) in a special issue of *Deep Sea Research*. The mean structure of the poleward California Undercurrent (CUC) along Pt. Sur was described by Collins et al. (2000). The existence and continuation of this flow along the California coast was shown by Pierce et al. (2000), while Noble and Ramp (2000) analyzed the spatial and temporal variability in the CUC. The latter study showed how and where the poleward flow is surface-intensified and how the variability is related to the surface wind stress. The separation of the surface upwelling jets from the cape-like coast, which becomes a conduit for transferring fluxes across the shelf, was described by Barth et al. (2000).

The seasonality of the mesoscale evolution of the CCS based on altimeter-derived surface velocity fields was described by Strub and James (2000). Eddy statistics such as eddy kinetic energy (EKE), wavelengths of meanders and jets and their spatial extents were, for the first time, quantified. Two very important questions were raised by Strub and James (2000): one related to the formation and westward migration of the seasonal jet and the other related to the source of fresh water within the CC core. They hypothesized that the seasonal jet begins as one or more local upwelling-front jets which move offshore as Rossby waves. These jets merge offshore (to about 130°W) to become a free, open-ocean jet that maintains its identity as the CC core during spring and summer. Based on previous observation and models, Strub and James (2000) also hypothesized that the source of the fresh water in the core of the CCS has multiple contributions such as waters from the North Pacific Current, coastal

inputs from the Columbia River, the Strait of Juan da Fuca and the British Columbia coast (sub-arctic origin).

In a high-resolution (5–10 km) analysis of hydrographic data along line 67 during the period 1988–2002, Collins et al. (2003) observed the California Current jet at about 100–200 km offshore near Monterey Bay. Their analysis suggests that the "mean" CC jet is at the inshore edge of the broader mean seasonal equatorward flow of the California Current. The mean jet's maximum velocity (6–10 cm/s) is much weaker than that of the jet (50–100 cm/s) identified by Brink et al. (1991). One interpretation is that the average currents over the 50-km or so mean CC jet width are on the order of 10 cm/s, but that much higher speeds are found in the narrow frontal regions within the CCS (Chavez, personal communication).

More recently, Belkin et al. (2009) carried out a frontal mapping characterization of the CCS based on available SST. Their frontal mapping for July 1985 and December 1985 (see their Figure 14) showed a dramatic change of scale (an order of magnitude) from summer to winter. The near-chaotic (disorganized and almost homogeneous) distribution of fronts in the summer changes in winter to an organized long-filament (∼1000 km) frontal distribution with gaps in between. This pattern is also observed in other eastern boundary current regions and is indicative of the prevalence of transitional and short-lived fronts associated with swift dynamical processes with time-scales of 1–10 days. This idea supports the Mooers and Robinson (1984) construct of meandering jets and filaments interacting with eddies and upwelling regions forced by large-scale and mesoscale atmospheric winds. A more recent overview of the processes in the CCS is presented by Barth and Checkley (2009).

Modeling and assimilation to understand the complex processes in the larger California Current region have been a major focus of many investigators, including McWilliams (1985), Miller et al. (1999), Marchesiello et al. (2003), Penven et al. (2006), Capet et al. (2008a,b,c), Moore et al. (2009) and others listed in these papers. During 2003 and 2006, major experiments were conducted in the coastal region of Monterey Bay (around the middle of the coastal zone), revealing some of the faster upwelling dynamical processes and their interactions with larger-scale features including offshore eddies, the CUC and coastal trapped waves (e.g., Ramp et al., 2009, this issue; Chao et al., 2009; Haley et al., 2009; Shulman et al., 2009).

It is clear from the above overview that this region is dynamically complex and rich with short-term energetic phenomena. Thus, it is important to (i) develop a systematic description of the system elements and (ii) characterize and document their scales and variability for possible use in modeling, initialization, validation and assimilation in a numerical prediction system.

## 3. Features, scales and variability in the CCS

Based on the above overview, we identified the following key points to be considered for a multi-scale synthesis of features: (i) the synoptic state would be able to sustain a frontal jet of speeds similar to those found by Brink et al. (1991); (ii) the low-salinity core of the CC might be influenced by these southward-flowing coastal jets mixing with the mean equatorward flow system (which is part of the large-scale subtropical gyre); (iii) offshore of Monterey Bay at around 36.5°N, the instantaneous jet (of Strub et al., 1991) and the mean current (of Collins et al., 2003) are within one degree of longitude of each other; and (iv) the addition of a number of eddies might provide a more stable configuration.

Below, various aspects of the multiscale variability of the prevalent circulation features in the CCS are summarized focusing on the summer (July–August) season. Some of these features can be seen in Figure 3 of Strub et al. (1991), which depicts surface pigment concentration from the CZCS satellite data from June 15, 1981. The characteristic CCS surface features are similar in SST and color images (Strub and James, 2000). The features studied and characterized here are: (i) the California Current (mean and its core jets); (ii) the California Undercurrent; (iii) the Inshore Countercurrent (Davidson Current); (iv) the coastal transition zone that separates the shelf circulation from the offshore flows; (v) the eddies; (vi) the anomalous pools of cold and fresh water; (vii) the baroclinic jets along upwelling fronts; (viii) the filaments; (ix) the squirts; and (x) the mushroom heads.

In particular, a comprehensive synthesis is provided of the typical widths, locations (distance from the coast), vertical extents, and basic characteristics of these features. The dominant spatial and tem-

**Table 1**
Characteristics of the synoptic features for the California Current System.

| Feature | Location | Width (km) | Vertical extent (m) | Characteristics and variability | Represented by |
|---|---|---|---|---|---|
| California Current (Equatorward flow) | 100–150 km offshore | 100–1350 | 0–500 | Baroclinic jet, $V_{max}$ = 50–70 cm/s, wavelength = $O$ (300 km) time-scale = 5–10 days | Mean flow (wide front) or climatology |
| CC core | 500 km offshore | 100 | 160 | Low-salinity parabolic pool | Parabolic isohalines with a core signature |
| CUC/inshore current (poleward flow) | 10–200 km offshore | 20–200 | 0–1000 | Core @ 200–275 m depth $V_{max}$ = 15–20 cm/s | CalCOFI data from July 1984 |
| Coastal transition zone | Continental slopes | | | Filaments, eddies, upwelling fronts and anomalous pools | Water-mass melding |
| Coastal eddies | C. Mendocino and Pt. Arena | <100 km | <300 | Low T, hi S and hi nutrient; time-scale = 40–60 days | Asymmetric eddies |
| Coastal jets along upwelling fronts | Over the shelf | 10–40 km | Above halocline ($\sigma_\theta$ = 26.5) | $V_{max}$ =100 cm/s, O (week) | Frontal water-mass structure |
| Anomalous pools | Onshore side of upwelling fronts | 20–30 km | <60 | Low $T$ and low $S$, time-scale = O (week) | Eddy structure |
| Large filaments | Up to 200 km offshore, and near Pt. Arena | <100 km | 100 or below | Low $T$ (12–13 C) and hi $S$ (32.7–33 psu), time-scale = 2–4 weeks; vertical velocity = −25 to 40 m/day | Weak frontal structure |
| Smaller filaments (squirts) | Onshore of upwelling fronts | 30 and 50–100 km long | Near surface | Low $T$ (10–12 C) and hi $S$ (>33 psu); time-scale = 6–10 days | Strong frontal signature |
| Mushroom heads (eddy dipoles) | Offshore in the CTZ | T-shape | Above seasonal thermocline | Ageostrophic and asymmetric, time-scale = 1–5 days | Asymmetric eddies and a front |

poral scales of variability of each of these features are identified from past observational, theoretical, and modeling analyses (Table 1). Some of these features are discussed below.

### 3.1. The California Current

The present understanding is that the core of the CC is at the inshore edge of the current. This low-salinity core is associated with the separating coastal jet (Barth et al., 2000) at the surface. This frontal jet also meanders and develops eddies as it progresses southward and interacts with the onshore upwelling regions and their filaments. The low-salinity core may have been first described by Lynn and Simpson (1987). They defined three cross-shore zones based on the seasonal signal in the dynamic height field from the CALCOFI data. A minimum in the dynamic height field occurred during the winter in the offshore region due to cooling. A maximum in the dynamic height field, caused by

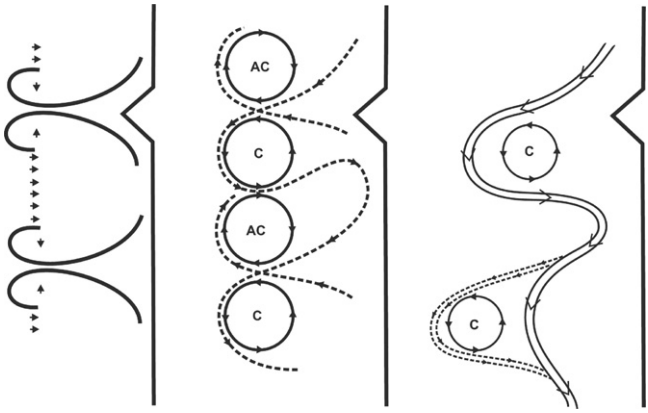


**Fig. 2.** The three simple conceptual models considered for the flow structure associated with the cool filaments (Strub et al., 1991): Squirts (left), mesoscale eddy field with cyclonic (C) and anticyclonic (AC) rotations (middle) and meandering jet (right).

currents, occurred in the nearshore zone during the winter. Eddies dominated the transition zone in between, where the standard deviation of the dynamic height was high, although its seasonal signal was relatively small. The core of the CC lies in this transition zone band. This relationship is also consistent with the Strub et al. (1991) description of the jet flowing through the field of eddies (see Fig. 15 of LS87).

A synergistic set of three simple model alternatives proposed by Strub et al. (1991, their Figure 1) for the flow structure of cool filaments is examined here (Fig. 2). As the first alternative, the idealized squirt is generated by nearshore convergences, such as those caused by local wind relaxations around capes, so the squirts have an onshore energy source. As the second alternative, the field of mesoscale eddies could draw recently upwelled water away from the coast, which has an offshore energy source. As the third alternative, a continuous southward jet meandering offshore and onshore was envisioned. This jet may entrain coastally upwelled water and pull it offshore. While all of the preceding alternatives may contribute to squirt formation, the third alternative of meander-eddy-upwelling is becoming the prevailing view of the CCS in spring/summer (see also Ramp et al., 2009; Pringle and Dever, 2009).

In a larger context, the meander-eddy-upwelling system as initially proposed by Mooers and Robinson (1984), and adapted here in Fig. 3, as a basis for synthesis of multiscale elements, should be able to reproduce realistic jets, eddies and squirts in a dynamical modeling framework. The schematic in Fig. 3 shows the complexity in the meander-eddy-upwelling system of the California Current off Oregon and California in the spring/summer. The coastal jet coming from the north moves offshore as the season progresses (denoted by the March, May, and July lines), and contributes downstream to the low-salinity core of the California Current. This core delineates the higher variability region nearshore from the less active regions offshore. The offshore region consists of the mean southeastward flow of the wind-driven subtropical gyre. The inshore region is populated by upwelling centers concentrated near the capes. Eddies generated by the meandering jet are found in both regions, and may exhibit either cyclonic or anticyclonic rotation. Temporally transient eddies of various sizes also occur.

### 3.2. The California Undercurrent (CUC)

The availability of synoptic-scale data for the CUC is sparse. Differences in periods of analysis, geographical coverage, and lack of high-resolution surveys challenge attempts to pinpoint the location and behavior of this feature. Early studies using current meters (Wickham et al., 1987; Huyer et al., 1989) established the existence of CUC. It was also shown to be warm, high-salinity and low-oxygen water at intermediate depths next to coast (Lynn and Simpson, 1987). Lagrangian float analysis unambiguously showed a continuous path of the CUC along the 200 m isobaths for about 440 km between San Francisco (37.8°N) and St. George Reef (41.8°N) during summer of 1993 (Collins et al., 1996). A

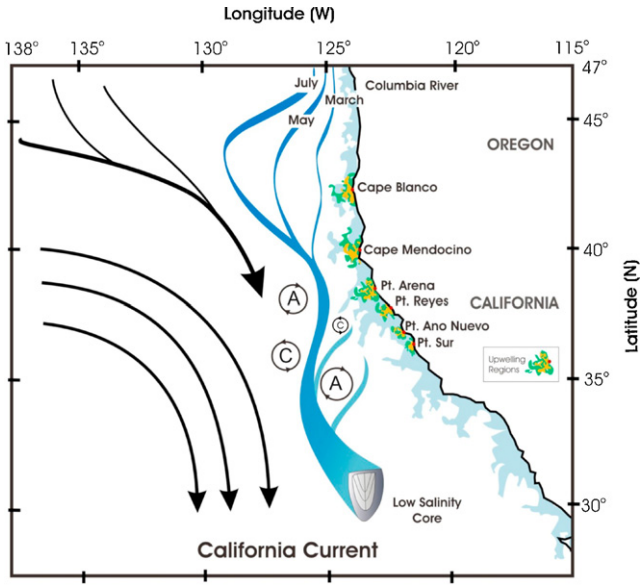


**Fig. 3.** This schematic shows the complexity in the meander-eddy-upwelling system of the California Current off Oregon and California in the spring/summer. The coastal jet coming from the north moves offshore as the season progresses (denoted by the March, May, and July lines), and contributes downstream to the low-salinity core of the California Current. This core delineates the higher variability region nearshore from the less active regions offshore. The offshore region consists of the mean southeastward flow of the wind-driven subtropical gyre. The inshore region is populated by upwelling centers concentrated near the capes. Eddies generated by the meandering jet are found in both regions, and may exhibit either cyclonic or anticyclonic rotation. Temporally transient eddies of various sizes also occur.

follow-up survey (Pierce et al., 2000) of 105 shipboard ADCP velocity sections during July to August 1995 found that, on monthly average, the CUC has a core speed of >10 cm/s from 200 m to 275 m depth at 20–25 km off the shelf break. These sections and the core path are available from the website http://diana.oce.orst.edu. Later, based on Lagrangian drifter analysis, the CUC was observed at 200 km offshore of Monterey Bay and at depths of 750–1000 m (Rischmiller, 1993; Garfield et al., 1999). Recent observations of the undercurrent are being analyzed to generate more understanding of the CUC for a future publication (Pierce, personal communication), which will be incorporated into a later version of this FM.

### 3.3. *The coastal upwelling regions*

Seasonal variations in the wind direction result in different circulation regimes along the coast of California at different times of year. From approximately March through September, prevailing southeastward winds combined with the effect of the earth's rotation, driving surface waters offshore, leading to coastal upwelling. The cool nutrient-rich waters upwelled from depth are responsible for the high primary productivity of California's near-shore region (Largier et al., 2006). The timing of the onset and cessation of the upwelling season varies somewhat with latitude. Within the upwelling season, there are numerous intermittent short periods, known as relaxations, when upwelling ceases due to weakened equatorward or poleward winds. Two August relaxations are described by Ramp et al. (2005) and Rosenfeld et al. (1994). The most intense coastal upwelling regimes are found around the many capes (e.g., Fratantoni and Haddock, 2009). The predominance of upwelling activity subsides in September, when the persistent strong northwesterly winds weaken, allowing a reversal in the coastal ocean to northward flow at the surface, called the Inshore Countercurrent or the Davidson Current. In the northern part of the region considered here, downwelling-favorable winds prevail through the fall and winter months, while in the southern region the winds are fairly calm during autumn, and are

highly variable in strength and direction during winter. Haley et al. (2009) reported four-dimensional simulation studies of dynamical processes, including upwelling in the Monterey region, while Ramp et al. (this issue) compared different simulations of such dynamics, pointing to the importance of model resolution and of longer coastal waves.

The inshore region of the CTZ is complicated by the poleward flow being interrupted by the summer upwelling jets flowing equatorward near the mouth of Monterey Bay (Collins et al., 2003). The water-mass characteristics of Monterey Bay during the upwelling and relaxation periods (Warn-Varnas et al., 2007) were used for constructing the upwelling FM profiles near Pt. Año Nuevo and Pt. Sur. For the development of the FORMS for the CCS region during summer, the present study is focused on the six upwelling regions around the six capes within the geographic region of interest: Cape Blanco, Cape Mendocino, Pt. Arena, Pt. Reyes, Pt. Año Nuevo and Pt. Sur. Note that one of the most productive places along the California coast, the Pt. Conception upwelling center, has been excluded from this study as it falls south of the domain; however, it could have been feature-modeled in a manner very similar to the other upwelling regions, had the domain been extended. Furthermore, recent studies suggest that Ekman pumping from local wind stress curl, which is enhanced adjacent to and southward of the coastal promontories, can be as important as Ekman transport from alongshore winds (Pickett and Paduan, 2003).

### 3.4. Other mesoscale features in the CCS region

During fall and winter, when the upwelling is not present, the Inshore Countercurrent (Davidson Current) has two distinct cores, one on the coast and one 50 km offshore (Collins et al., 2003). Since the present focus is on the development of CCS-FORMS for the summertime, the development of these features is deferred. Coastally trapped waves (CTW) are another type of feature that is excluded. Dynamical FMs based on CTW modes (Brink, 1982) which resolve the proper phases based on real-time wind information will be the subject of a later study. The CCS also experiences river input during all seasons. However, for this summertime development, river inputs are arguably inconsequential except for the Columbia River, which has not been included in this study. River inputs can be feature-modeled following the existing Chesapeake Bay outflow FM (Gangopadhyay et al., 2005). Apart from these features, there are also very energetic and important shallow water (<100 m) features in the CTZ around the coastal region of Monterey Bay and the CCS. The filaments, coastal eddies, anomalous pools of cold water, jets along the upwelling fronts, squirts across the shelf, and mushroom-like vortex pairs are critical to reproduce for accurate forecasting. The scales and variability of these features have been identified (Table 1), and relevant references are cited (Table 2).

These features, such as filaments, jets, and mushroom-vortices, are related to specific dynamical processes, including instability, upwelling and wind-driving. It has been proposed that subduction plays a very important role inside the filaments, forcing these cool filaments downwards, below the ambient warm surface waters (Brink et al., 1991). The mushroom vortices are generated only if certain conditions of the flow field are met (Mied et al., 1991).

Standing eddies, a number of which are known to exist in the CCS, including some in our study domain (near Heceta Bank, Pt. Arena, and Pt. Mendocino), were not explicitly included in this study. Others, such as in the Santa Barbara channel and the Juan de Fuca region, are outside of the geographical domain of interest. While these eddies are not included in this study, inclusion at a later stage of development would follow the existing formulation for symmetric (Gangopadhyay et al., 1997) and asymmetric (Calado et al., 2006) eddy FMs.

Many of these mesoscale, submesoscale and finer-scale features are generated by non-linear interactions of the CC, CUC, upwelling, and eddies with background circulation and with one another. They occur when certain ambient conditions are met in terms of forcing, boundary conditions and stratification. For example, CTWs are generated from a dynamical interaction between winds, topography and coast; standing eddies need a topography constraint; squirts, filaments and jets might need upwelling, instability of fronts, eddy driven intrusions, capes, and promontories, etc., in addition to wind driving.

For this first implementation of FORMS for the CCS, such complications have been excluded. However, as will be shown later, once the primary features are in place, the ensuing model integration generates mesoscale and submesoscale features such as filaments and mushroom vortices. Examples

**Table 2**
Reference list (not exclusive) for the studies that were used to study and select parameter ranges for the different features.

| Features | References |
|---|---|
| California Current (mean and its baroclinic jet core) | Brink et al. (1991), Chelton (1984), Chereskin et al. (1998), Collins et al. (2003), Kelly et al. (1998), Lynn and Simpson (1987), Lynn et al. (1982), Miller et al. (1999), Ramp et al. (1997a,b), and Tisch et al. (1992) |
| Poleward flow (California Undercurrent and Inshore Davidson Current) | Chavez et al. (1997), Collins et al. (1996, 2000, 2002, 2003), Garfield et al. (1999), Huyer et al. (1998), Marchesiello et al. (2003), Noble and Ramp (2000), Oey (1999), Pierce et al. (2000), Ramp et al. (1997a,b), Swenson and Niiler (1996), Wickham (1975), and Wooster and Jones (1970) |
| Coastal transition zone (CTZ) | Brink et al. (1991), Brink and Cowles (1991), Chelton and Schlax (1991), Haidvogel et al. (1991), Haynes and Barton (1991), Kosro et al. (1991), Marchesiello et al. (2003), Strub et al. (1991), and Walstad et al. (1991) |
| Coastal eddies | Bucklin (1991), Hayward and Mantyla (1990), and Hickey (1998) |
| Coastal jets along upwelling fronts | Allen et al. (1991), Chavez et al. (1997), Huyer (1983), Huyer et al. (1991), Pierce et al. (1991), Kosro et al. (1991), Rosenfeld et al. (1994), Smith and Lane (1991), Strub et al. (1991), Tracy (1990), Washburn et al. (1991) |
| Anomalous pools | Hayward and Mantyla (1990) and Strub et al. (1991) |
| Large filaments | Abbott and Barksdale (1991), Abbott and Zion (1987), Bernstein et al. (1977), Brink et al. (1991), Chavez et al. (1991), Chereskin and Niiler (1994), Dewey et al. (1991), Flament et al. (1985), Haidvogel et al. (1991), Kadko et al. (1991), Mackas et al. (1991), Ramp et al. (1991), Strub et al. (1991), and Traganza et al. (1980, 1981) |
| Squirts (smaller filaments) | All of the above, specially Dewey et al. (1991), Hickey (1998), and Ramp et al. (1991) |
| Mushroom heads | Ikeda and Emery (1984), Mied (1990), Mied et al. (1991), Munk et al. (2000), Sheres and Kenyon (1989), and Smith and Lane (1991) |

of such realistic simulations have been given recently for the southwestern Atlantic region (Calado et al., 2008).

## 4. Feature models for different features in the CCS

A prerequisite synthesis of the prevalent features in the CCS was presented in Section 3 and their spatial and temporal scales are summarized in Table 1. In particular, the typical width, location (distance from the coast), vertical extent, and core characteristics of these features have been investigated. The CCS-FORMS are restricted here to a combination of the CC, CUC and upwelling FMs in a climatological background circulation for initialization. Eddies can be added in a short-term forecasting system, and multiple examples of such eddy FMs exist in earlier studies (Gangopadhyay and Robinson, 2002; Calado et al., 2006, 2008; and others). In this section, the FMs that were developed based on previous studies are presented for a subset of those features in this first application to numerical modeling.

### *4.1. Feature models for the California Current and its low-salinity core*

The schematic in Fig. 3 shows the arrangement of different features in the CCS region. From a synoptic-scale viewpoint, the California Current mean flow has a meandering jet structure at its core. The low-salinity pool in the core of the CC has been chosen as the primary characteristic, and an FM has been developed for this structure. Low salinity is a reasonable descriptor for the path of the CC (see Figures 9 and 11 of Lynn and Simpson, 1987). The salinity minimum is offshore of the velocity maximum, which may be due to more mixing with inshore waters than with offshore waters (Lynn and Simpson, 1987).

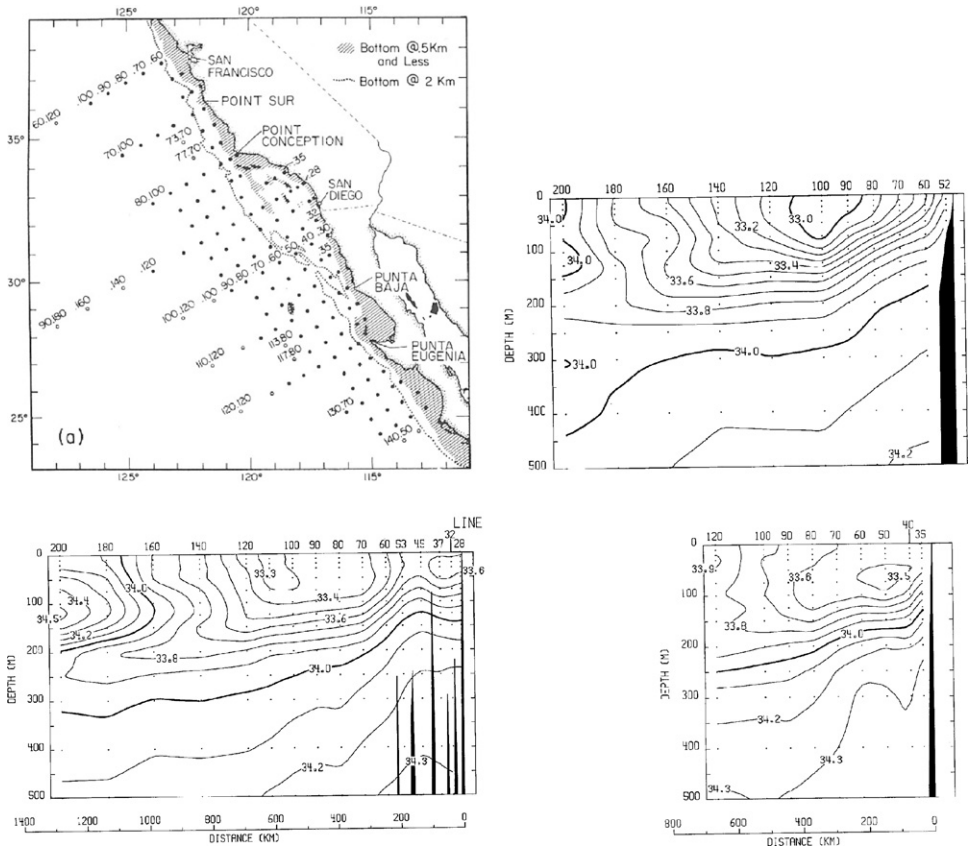


**Fig. 4.** (a) The CalCOFI station locations along different lines (from Lynn and Simpson, 1987); (b), (c) and (d) are the vertical sections of mean salinity for the month of July along CalCOFI station lines 60, 90 and 110 (from Lynn et al., 1982), respectively. Note the consistency of the low salinity pool in these sections.

Based on the vertical sections of mean salinity for July along CalCOFI stations 60, 90 and 110 (Fig. 4), the low-salinity pool occurs in these sections as a distinct core. The isohalines in the low-salinity core are represented by a series of parabolas having their foci on the same vertical (see Fig. 5a). This vertical line passes through the center of the core, is the axis of all the parabolic isohalines, and is perpendicular to the directrix of the set of parabolas.

The parabolic formulation for the low-salinity pool for a point $(x, z)$ (Fig. 5a) is given by

$$x^2 = 4a(z + H) \tag{1}$$

where $H$ is the depth of the isohaline core, and the parabolic isohaline has vertex at $(0, -H)$ in the $x$–$z$ plane (Fig. 5a).

At the surface, where $z = 0$, the salinity data (obtained by Lynn et al., 1982, and presented by Lynn and Simpson, 1987) was used for evaluating the "$a$" values of the parabolic isohalines. Specifically, for the surface points of each parabolic isohaline, a simple relationship between the maximum width ($W$) of the pool and the depth ($H$) of the isohaline is: $(W/2)^2 = 4aH$; which leads to $a = (1/H)(W/4)^2$. Using the observed width and depth of each of the isohalines for each of the sections in Fig. 4, the "$a$" values of these parabolas were obtained (Table 3). The modeled parabolic isohalines corresponding to Line 60 (Fig. 5b) are comparable to the observed isohalines (Fig. 4b).

The "core" area of the pool and the parabolic isohalines outside the core are next distinguished. The salinity in the core area is assumed to be constant, $S_0$, from the surface to the core depth ($C_0$)

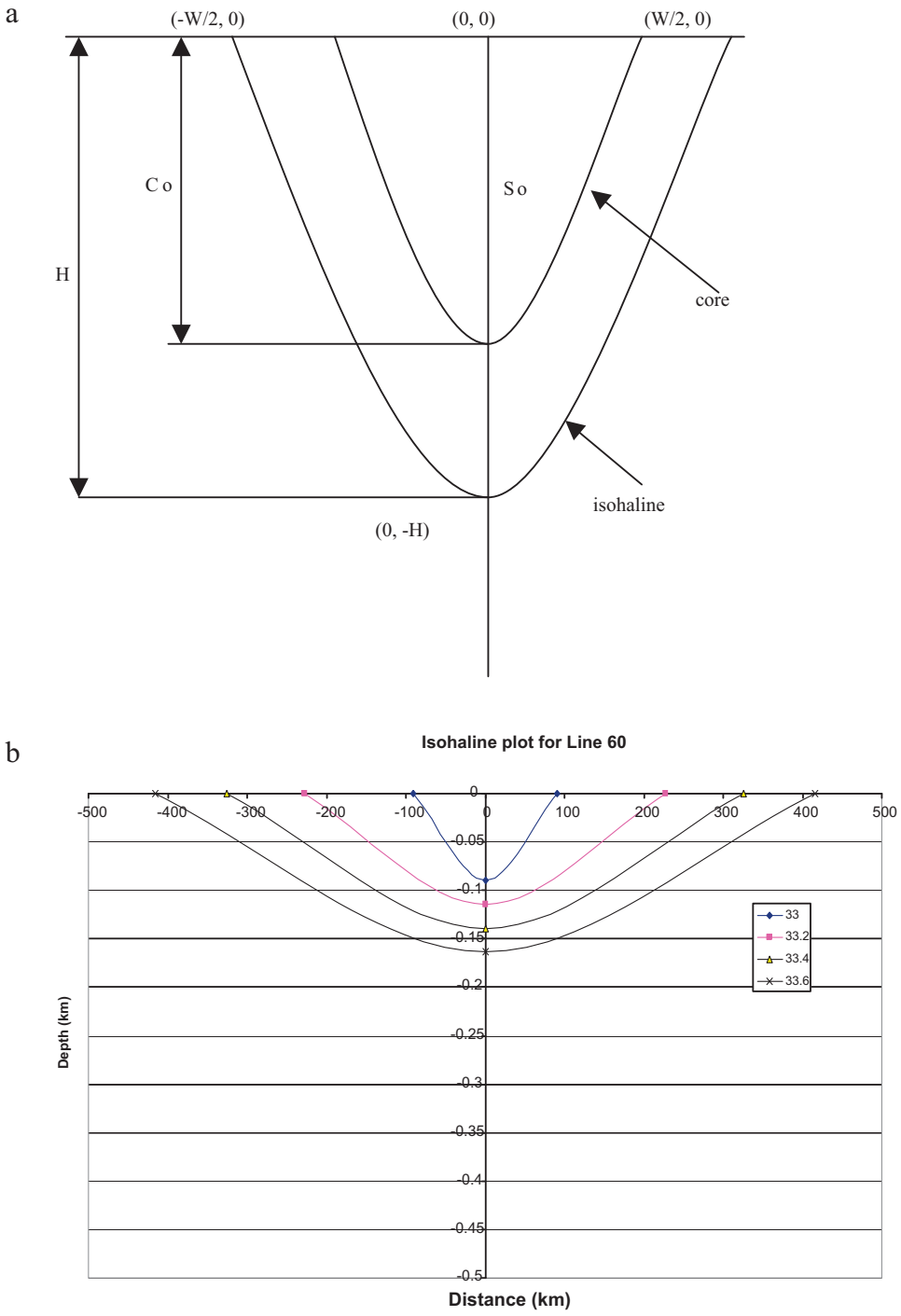


**Fig. 5.** (a) Schematic representation of a parabolic isohaline for the low-salinity pool feature model; (b) feature modeled vertical section of salinity at line 60.

**Table 3**
Parameter values for the low-salinity pool parabolic feature model.

| | Salinity (psu) | Max core width (km) | Depth (m) | $a$ (km) |
|---|---|---|---|---|
| Line 60 | 33 | 180 | 90 | 22,730 |
| | 33.1 | 340 | 103 | 70,200 |
| | 33.2 | 455 | 115 | 112,970 |
| | 33.3 | 557 | 127 | 152,810 |
| | 33.4 | 651 | 139 | 190,740 |
| | 33.5 | 745 | 151 | 229,970 |
| | 33.6 | 832 | 163 | 265,575 |
| | 33.7 | 940 | 175 | 316,100 |
| Line 90 | 33.3 | 80 | 68 | 5825 |
| | 33.4 | 405 | 100 | 102,650 |
| | 33.5 | 506 | 126 | 127,290 |
| | 33.6 | 608 | 150 | 153,975 |
| | 33.7 | 724 | 174 | 188,115 |
| Line 110 | 33.6 | 383 | 110 | 83,585 |
| | 33.7 | 528 | 120 | 145,360 |
| | 33.8 | 644 | 135 | 192,055 |

bounded by the parabolic isohaline of $S_0$ in the $x$–$z$ vertical section. Thus, from a FM perspective, given a specific set of $S_0$ and $C_0$ values, the salinity at each point outside the "core" within the pool needs to be determined. Eq. (1) above defines the boundary of the core.

As above, the parabolic assumption allows evaluation of the "$a$" value for different "$H$" and plotted. Then, "$a$" is observed to increase almost linearly with "$H$", which led to relating '$H$' and '$a$' by the following equation

$$H = \left(\frac{\partial H}{\partial a}\right)(a) + C_0 \tag{2}$$

where $C_0$ is the core depth.

Substituting this value of $H$ in Eq. (1), then

$$x_1^2 = 4a\left[z_1 + \left(\frac{\partial H}{\partial a}\right)(a) + C_0\right].$$

Rearranging terms, a quadratic in "$a$" can be formed

$$\left(\frac{\partial H}{\partial a}\right)(a^2) + (z_1 + C_0)(a) - \left(\frac{x_1^2}{4}\right) = 0$$

whose real solution is given by:

$$a = \frac{-(z_1 + C_0) + [(z_1 + C_0)^2 + (\partial H/\partial a)(x_1^2)]^{1/2}}{2(\partial H/\partial a)} \tag{3}$$

Thus, once '$a$' is obtained, Eq. (2) is used to determine the depth, $H$, of the isohaline. In this way, the isohaline is constructed. Analysis of the observed core (from Fig. 4) at several lines yielded an almost constant value of $(\partial S/\partial a)$. Thus, similarly to $H$ of an isohaline, pointwise salinity can now be obtained from

$$S = \left(\frac{\partial S}{\partial a}\right)(a) + S_0 \tag{4}$$

where $S_0$ is the salinity of the core of the pool. Thus, it turns out that $S$ can be expressed as a function of $S_0$, $C_0$, $\partial S/\partial a$ and $\partial H/\partial a$. Given these four variables, the salinity (using Table 3, Eqs. (3) and (4)) can be determined at any point in the low-salinity pool.

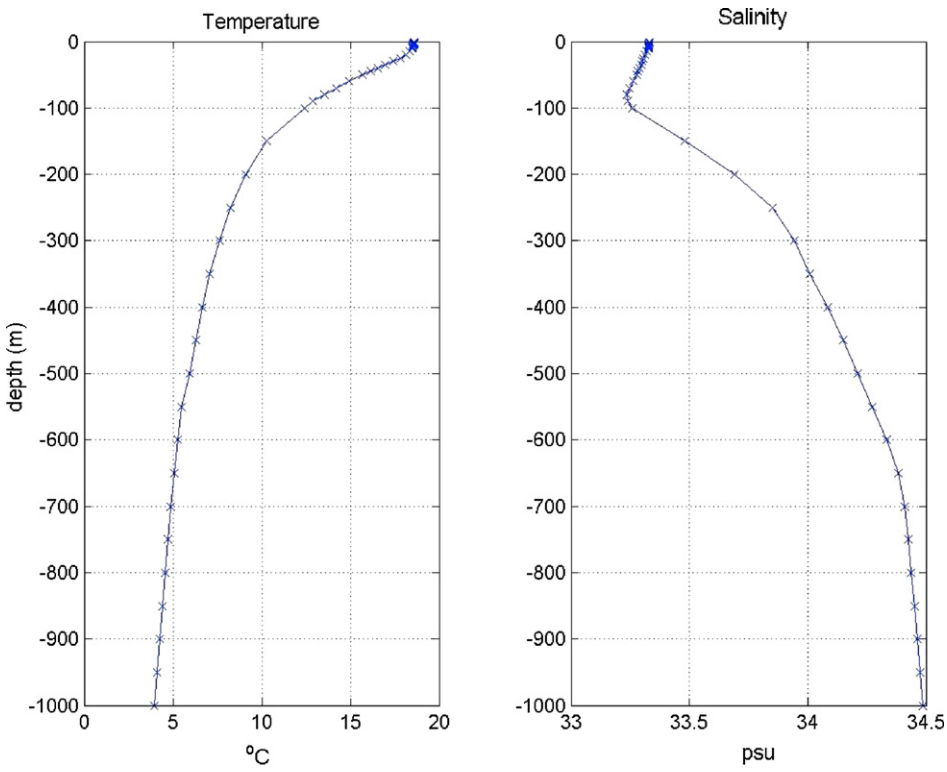


**Fig. 6.** The temperature and salinity profiles for the California Current Core.

The temperature and salinity profiles for this core (Fig. 6) were adapted from Lynn and Simpson's (1987) analysis of the data obtained through the long-term monitoring program called CalCOFI. From such a typical salinity profile, the variables $S_0$ and $C_0$ can be extracted for the FM. The salinity and depth variation with "$a$" are given by the numbers in Table 3. For the implemented FM, the initial path of the CC is a representative one, and would have to be obtained on the basis of SST or color signatures. It is suggested that the core of the CC is better identified from color images (such as those from MODIS) as the chlorophyll boundary (Smith et al., 1986). In the future, when the sea surface salinity fields will be available from satellites at high-enough (∼10–20 km) resolution, one would expect to identify this core of the CCS on a regular basis.

### 4.2. Feature models for the California Undercurrent (CUC)

The scarcity of data for the CUC was highlighted in the overview section. The only complete and continuous profile mapping was done by Pierce et al. (2000) (Fig. 7). It is, however, worthwhile to note that the location of the CUC offshore of Monterey Bay (this region being the focus of AOSN-II during summer 2003) was highly variable. Early observations of the CUC in this region (36–37°N) (Wickham, 1975) indicated a complex alongshore flow near the coast, in both poleward and equatorward directions in the upper 500 m offshore close to 123°W. In particular, a poleward flow was subdivided into two parts by a strong (60 cm/s) equatorward jet down to 500 m (Figure 11 of Wickham, 1975). The NMFS survey sections (Figure 2 of Pierce et al., 2000) indicate a maximum of the CUC shifted offshore at 36.47°N and at 36.8°N, while flowing very close to the coast north of 37°N (see Figure 4b of Pierce et al., 2000). A section at 35.97°N clearly has an equatorward jet in the middle of the weak poleward flow.

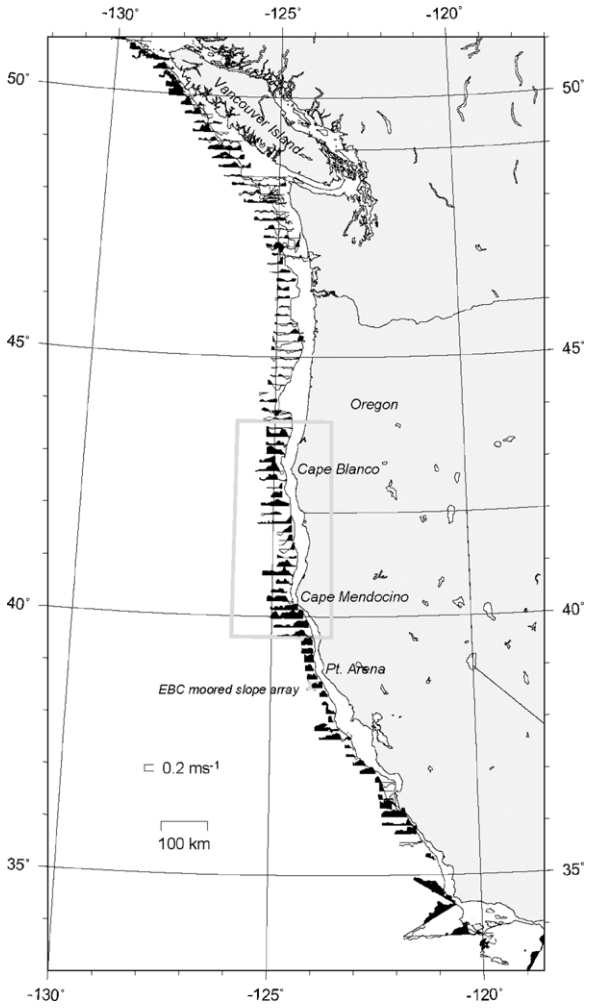


**Fig. 7.** Locations of ADCP sections and maximum speed and locations of the California Undercurrent (from Pierce et al., 2000). ADCP sections were made across the continental margin from 32 to 51N at about 20 km spacing during the 1995 upwelling season. The depth of the core of poleward flow at each section is determined by taking the center of mass (these depths range between 118 and 258 m). The vertical arrows show the speed and location of the maximum poleward flow found at this depth. The thick horizontal lines show the width of the poleward flow at half-maximum velocity. The whiskers show the full lengths of the ADCP sections.

In fact, the area of poleward flow off Point Sur can extend well beyond the upper continental slope up to a distance of 200 km from the coast (Rischmiller, 1993) and to a depth of 750–1000 m or greater (Garfield et al., 1999). Based on Lagrangian drifters during 1992–1995, the individual and ensemble spaghetti diagrams (Figures 5 and 6 of Garfield et al., 1999) clearly show that the CUC flow is further offshore across the Monterey Bay region than it is to the north.

With this background, the July 1984 CalCOFI data set (analyzed by Pierce et al., 2000) has been identified as a candidate analysis data set for forming the basis of a CUC template. A first-order FM for the CUC will be implemented on the basis of this data set from July 1984, and other supporting temperature-salinity observations. These FM profiles are shown in Fig. 8. Preliminary analysis suggests that a warm and saline water mass can be traced at 200–300 m depth. Interestingly, the path of this

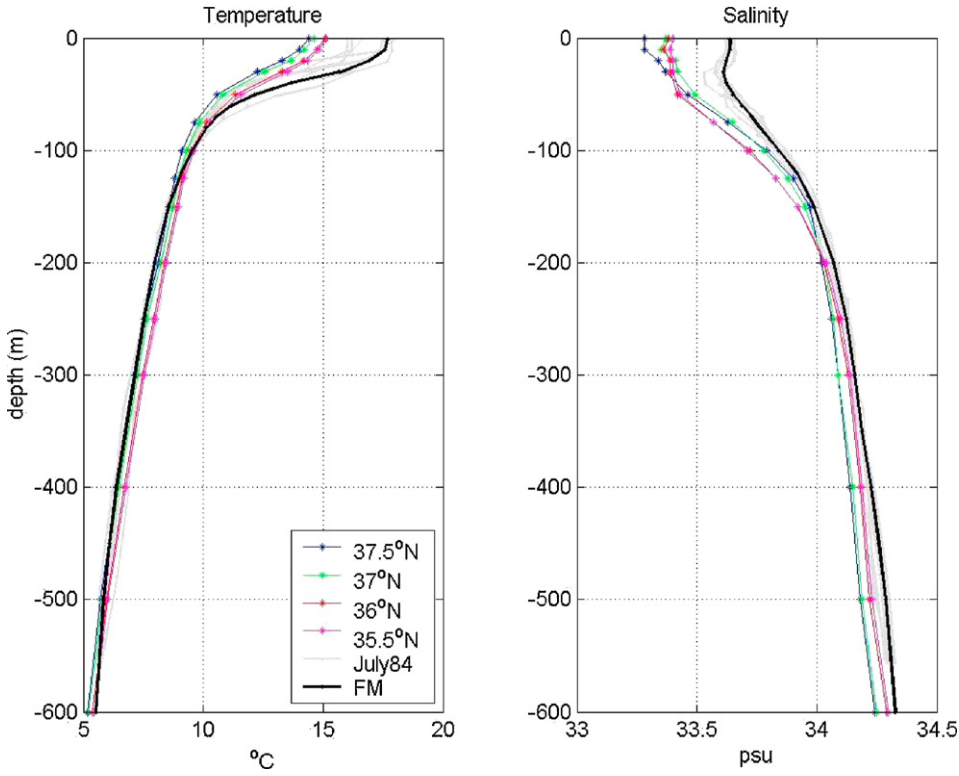


**Fig. 8.** The CUC-FM (black) profiles compared with observed (grey) and Levitus (color) profiles.

water mass follows the 2500-m isobath in the latitudinal range of 34–37.5°N. This offshore trajectory resembles a single drifter trajectory (Figure 6 of Garfield et al., 1999).

At depth, the CUC sheds eddies, as indicated by Garfield et al. (1999, 2001), tracking 38 approximately isobaric RAFOS floats ballasted at 300 m in the CUC. Two size-classes of eddies were found: small (radius < 35 km) rapidly rotating anticyclonically as submesoscale coherent vortices called "cuddies," and larger (radius > 50 km) eddies formed due to other processes such as baroclinic instability. The cuddies propagate westward into the interior with speeds of 1–2 cm/s (see Figure 5 of Garfield et al., 2001). It will be demonstrated later that the feature-modeled CUC develops eddies at subsurface depths during the dynamical simulations similar to those observed.

### 4.3. Coastal upwelling front feature model

This subsection documents the FMs of the coastal upwelling fronts. Six locations are chosen for the upwelling centers – Cape Blanco, Cape Mendocino, Pt. Arena, Pt. Reyes, Pt. Año Nuevo and Pt. Sur. As mentioned earlier, Pt. Conception is to the south of our domain and excluded here. However, it can also be feature-modeled following the methodology described next.

The development of upwelling FMs for each cape follows the methodology of Shaji and Gangopadhyay (2007). An upwelling FM requires the specification of two T and S profiles – an inshore profile and an offshore profile – which are dynamically interpolated with a $\tan h$ function (see Shaji and Gangopadhyay, 2007; Calado et al., 2008, for details).

The upwelling region's temperature is given by

$$T(\eta, z) = T_o(z) + [T_u(z) - T_o(z)]\, m(\eta, z) \tag{5}$$

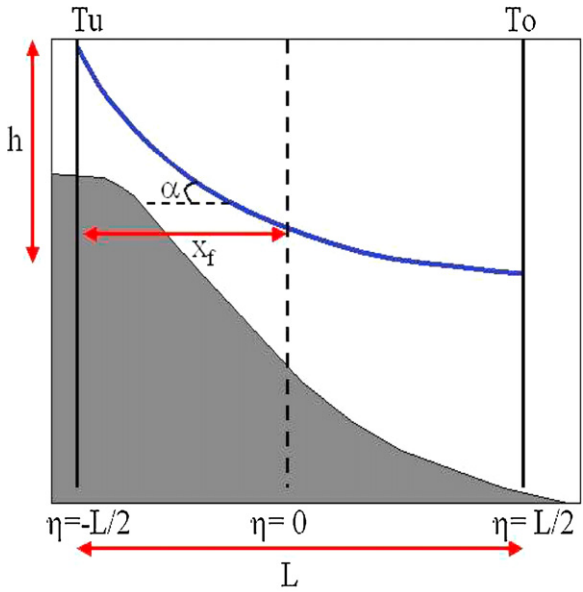


**Fig. 9.** A schematic of the upwelling feature model (after Calado et al., 2008). See text for the details of the parameter definition.

where

$$m(\eta, z) = \frac{1}{2} + \frac{1}{2}\tan h\left[\frac{\eta - \theta_z}{\lambda}\right]$$

is a melding function, $\eta$ is the cross-frontal distance from the axis of the front, and $z$ is positive vertically upward. $T(\eta, z)$ is the upwelling regional temperature distribution, $T_u(z)$ is the nearshore temperature profile, and $T_o(z)$ is the offshore temperature profile. $\theta_z$ is the slope of the front, and $\lambda$ is the e-folding half-width of the front (=$L$/2) (see Fig. 9).

Base data for the six upwelling regions were obtained from various sources and various cruises (Table 1 of Kim et al., 2007). Fig. 10 shows the newly generated FM temperature (Fig. 10a) and salinity (Fig. 10b) profiles for the coastal upwelling front at Cape Blanco. Fig. 10c is a $T/S$ diagram where inshore and offshore $T$ and $S$ (red) and derived FM $T/S$ profiles (blue) are compared to show the range captured by the FM. The resulting upwelling section at initialization is shown in Fig. 11. Clearly such initialization would have significant impact on the predictive capability of a forecast system in the shallow coastal region of the CCS. Similar constructs of the upwelling FMs were derived and implemented for the other five capes.

## 5. Multiscale initialization, model domain and numerical parameters

As indicated in Section 1, a feature-oriented methodology requires the development of a multiscale circulation template for the region. This "basis template" is designed from a feature-based synthesis of the regional circulation pattern. From it, is produced a map of dynamically strategic sampling locations for placing FM profiles, which provides the "synthetic synoptic expressions" for fronts, eddies, gyres, and other circulation structures and water masses at the initialization or model-updating phase. A suitable large-scale climatology is then selected to provide the background for the mesoscale features. Further, a multiscale objective analysis (OA; Lermusiaux, 1999a,b) is performed to meld the synoptic mesoscale and large-scale fields, which results in a three-dimensional field for initializing a numerical model grid. In this section, the initialization procedure is described, followed by details of the selected model domain and its numerical parameters.

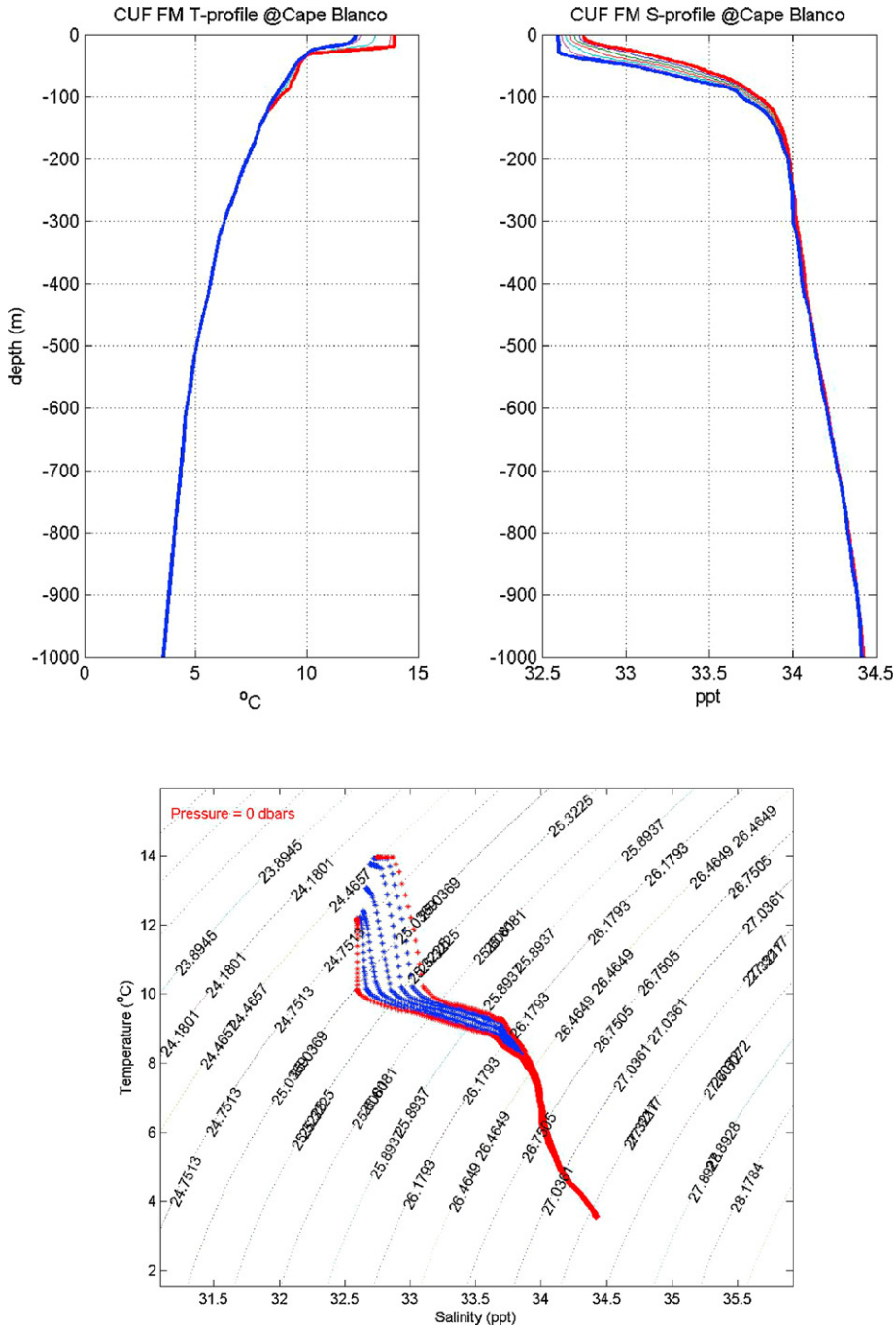


**Fig. 10.** Coastal upwelling front feature model T-profiles (left, a) and S-profiles (right, b) at Cape Blanco. Thick blue and red lines represent inshore and offshore profiles, superimposed on generated FM T&S along a transect. The bottom panel (c) shows the T/S diagram: inshore and offshore profiles in red and generated FM T/S profiles in blue at different offshore locations.

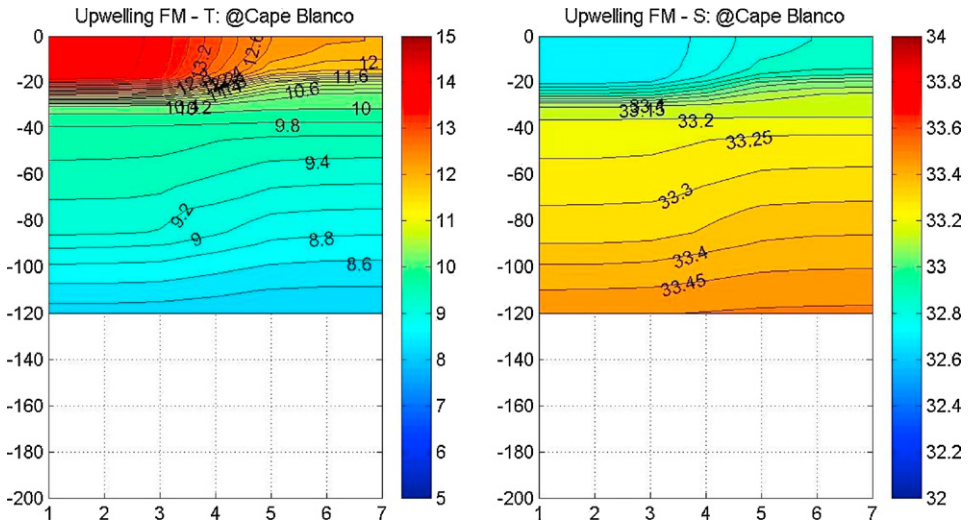


**Fig. 11.** Cross-section plots of feature model temperature (left) and salinity (right) off Cape Blanco.

### 5.1. Construction of a multiscale initialization using the feature-based synthesis

For synoptic forecasting, it is necessary to resolve the dynamic evolution of meanders, cross-frontal exchanges, eddy-frontal interactions, upwelling-jet-filament development, etc. The multiscale synoptic circulation template, which specifies the characterization of these features, ensures the presence of synoptic structures in the initialization and updating fields for nowcasting and forecasting. An example of this template is presented here for the CCS (Fig. 12). First, temperature and salinity FM fields are selectively sampled along and across the important features. The dots in Fig. 12 are the locations chosen to resolve the prevalent scale of each feature. Previous synoptic sections along and across feature locations are used to develop the strategic locations and to design the FMs. Second,

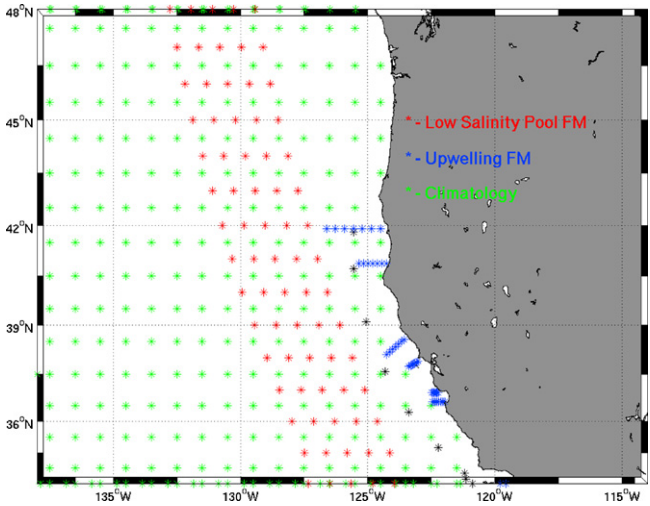


**Fig. 12.** Strategic sampling locations for the CC (red '*')- and CUC-FMs (black '*'), superimposed on the 1° Levitus (green '*') temperature in the surface layer together with the six upwelling sections (blue '*'). This figure defines the "basis-template" for the CCS-FORMS.

**Table 4**
Statistical parameters used for multiscale OA for initialization of the CCS region.

| Data type | Parameters | | |
|---|---|---|---|
| | Decay scale (km) ($x$/$y$) | Zero-crossing scale (km) ($x$/$y$) | Source data |
| Synoptic FMs | 50/50 | 300/300 | CCS, CUC, upwelling |
| Background field | 200/200 | 500/500 | Climatology |

these sampled fields are treated as pseudo-CTD observations and objectively analyzed with appropriate background seasonal climatology (green dots) of the region. The resulting multiscale field thus combines the synoptic structures in a background of appropriate climatology, ready for nowcasting and forecasting.

The details of designing a circulation template are explained for the Gulf of Maine/Georges Bank region by Gangopadhyay et al. (2003), and for the Brazil Current System by Calado et al. (2008). For the California Current, considerations must be given to (i) resolving the low-salinity pool at its core, (ii) maintaining a broad (500-km) width of the current along its path following the coastline, (iii) allowing for its interactions with the upwelling regions, and (iv) capturing the subarctic inflow to the geographic region of interest. The six upwelling regions are represented in their synoptic state with high resolution comparable to their radius of deformation (∼5 km). The CUC path is best resolved by strategically placing its FM profiles along the observed path (Pierce et al., 2000).

The major advantage in using such a template is the ability to resolve synoptic structure on the basis of past oceanographic knowledge of the region, even when there is a lack of observations for the synoptic features. Note that the CC low-salinity core is resolved by 5 stations (red stars in Fig. 12) of pseudo-CTDs across the CC jet at 15 sections along the path; the six upwelling regions are resolved by an inshore, an offshore and three in-between stations each (blue stars in Fig. 12); and the CUC is resolved by 5 across-current stations at 7 different alongshore locations (black stars in Fig. 12). These yield a total of about 150 stations to describe the synoptic behavior of this regional ocean. Note that the spacing along the currents would depend on the synoptic image (from satellite) and the meandering nature of the current (wavelength, measoscale evolution, etc.).

Once the FMs are developed (as described in Section 4), an initialization field is then generated by objectively analyzing the synthetic FMs on the circulation template in a selected background climatology for a multi-scale synthesis. The green stars in the circulation template (Fig. 12) are the locations of the Boyer et al. (2005) 1/4-degree climatology data. The multiscale OA is, in fact, done in two stages. In the first stage, the largest dynamical scales are resolved, using estimated large-scale e-folding spatial decays, zero-crossings and temporal decay. The background for the first stage OA is the horizontal average of the climatological data. In the second stage of the OA, the synoptic mesoscale phenomena are resolved using their estimated space-time scales. The relevant statistical parameters for the different scales are the same for all depths and are summarized in Table 4. The background for this OA is the first stage OA. Once the initialization field is available as a result of the multi-scale synthesis, any numerical model can then be used for nowcasting, forecasting, and dynamical process studies with such initialization fields.

Boyer et al.'s (2005) temperature and salinity fields were objectively analyzed for August with 1/4 degree of spatial resolution. The method of objectively analyzing the data is the same as outlined in Boyer et al. (2005) for temperature and salinity. There are differences in technique necessitated by the different scales of the analysis. In the one-degree analysis, the radius of influence is 250 km; in the quarter-degree analysis, the radius of influence is 40 km.

### 5.2. The POM parameters and domain setup

Initialization of any dynamical model requires the specification of each prognostic variable at each grid point of the three-dimensional model domain. In this work we chose the terrain-following coordinate system for this implementation of POM (Blumberg and Mellor, 1987; Ezer and Mellor, 1994, 1997). The domain consists of $150 \times 150$ grid points in the horizontal with 8-km resolution and 31

non-uniform vertical levels. The model domain is delineated geographically by 34.38°N, 48.82°N and −138.22°E, −118.68°E.

The model is based on the ETOPO5 data set. The depth range is 5–6000 m. Open boundary conditions were used on the north, south, and west. Along these boundaries, the model's thermohaline structure was held to initial temperature and salinity values via partially clamped boundary conditions (Blumberg and Kantha, 1985). Also, a radiation condition based on Summerfield's equation was applied to the baroclinic velocities on the open boundaries. The Flather radiation condition (Palma and Matano, 1998) was applied to the barotropic velocities, and a non-gradient condition for the free sea surface elevation was employed as well.

As a consequence of the relaxation in the temperature-salinity fields, a geostrophic flow was imposed at the model's open boundaries through the inclination of the isopycnal surfaces. In other words, the climatological signal, rendered by the inclinations of the isothermal and isohaline surfaces, contains the signal of both the velocity component generated by wind forcing and the component associated with the thermohaline circulation. The wind forcing was generated from the mean August field extracted from QuikScat data (Graf et al., 1998). The deep CUC, underlying the CC, was included in the initialization, and brought the influence of the thermohaline circulation component on the mesoscale activity in the region of interest.

### 5.3. Initialization strategy for short-term forecasting with POM

Short-term simulations require three-dimensional specifications of initial fields of $T$, $S$, $u$ and $v$. However, the standard practice for basin-scale numerical modeling exercises is to specify $T$ and $S$ only, with zero velocity (Ezer and Mellor, 1994, 1997; Mathew and McClean, 2005). The basin-scale approach requires models to develop the inertia fields in a one- to ten-year-long "spin-up" period. As mentioned earlier, the present goal is to develop a system for short-term forecasting where it is not feasible to run models over a long spin-up period or where an estimate of velocity from a feature-model is expected to be more accurate than zero velocity. Thus, specifying the best possible velocity field in addition to the mass ($T$ and $S$) field becomes mandatory for such short-term simulations. Of course, subsequent adjustment runs including wind forcing and baroclinic internal processes can still be necessary prior to forecasting. Such an approach has also been extended to initialize uncertainty fields (Lermusiaux et al., 2000; Lermusiaux, 2002) and to balance stochastic ocean forcing (Lermusiaux, 2006).

Previous work on such adjustment procedures included the Harvard Ocean Prediction System (HOPS) in the studies of Gangopadhyay et al. (1997, 2003) and Brown et al. (2007a,b), the Regional Ocean Modeling System (ROMS) by Shaji and Gangopadhyay (2007) and Kim et al. (2007), and a first application with POM by Calado et al. (2008). The set-up strategy for POM in the CCS region used climatological temperature and salinity initial fields following Ezer and Mellor's (1997) methodology, with the additional imposition of geostrophic velocity as the initial condition for the baroclinic velocities, balanced with the initial $T$–$S$ field. Specifically, the $T$ and $S$ fields were held fixed over the first five days of simulation in the diagnostic mode, an approach described by Ezer and Mellor (1997). These authors used this diagnostic mode, available in POM, to dynamically adjust the momentum field with the underlying mass field and bottom topography. A similar technique for initializing POM with geostrophic velocities was used by Castelao et al. (2004) to study shelf break upwelling in the region of southeastern Brazil. The initial geostrophic velocity was computed from the temperature and salinity by the OA methodology described by Lozano et al. (1996). Representative initial fields of surface temperature, salinity, and velocity are examined for day 1 (Fig. 13, top left, and Fig. 14, top left).

## 6. Dynamical simulations with feature models

The long-term goal of this study is to develop the capability for nowcasting and forecasting using the FORMS technique in the CCS region. So far, the development of a set of appropriate FMs for this region and their incorporation into a multiscale objectively analyzed initialization has been discussed. In this section the results of a 40-day simulation with such initialization using the POM setup are presented,

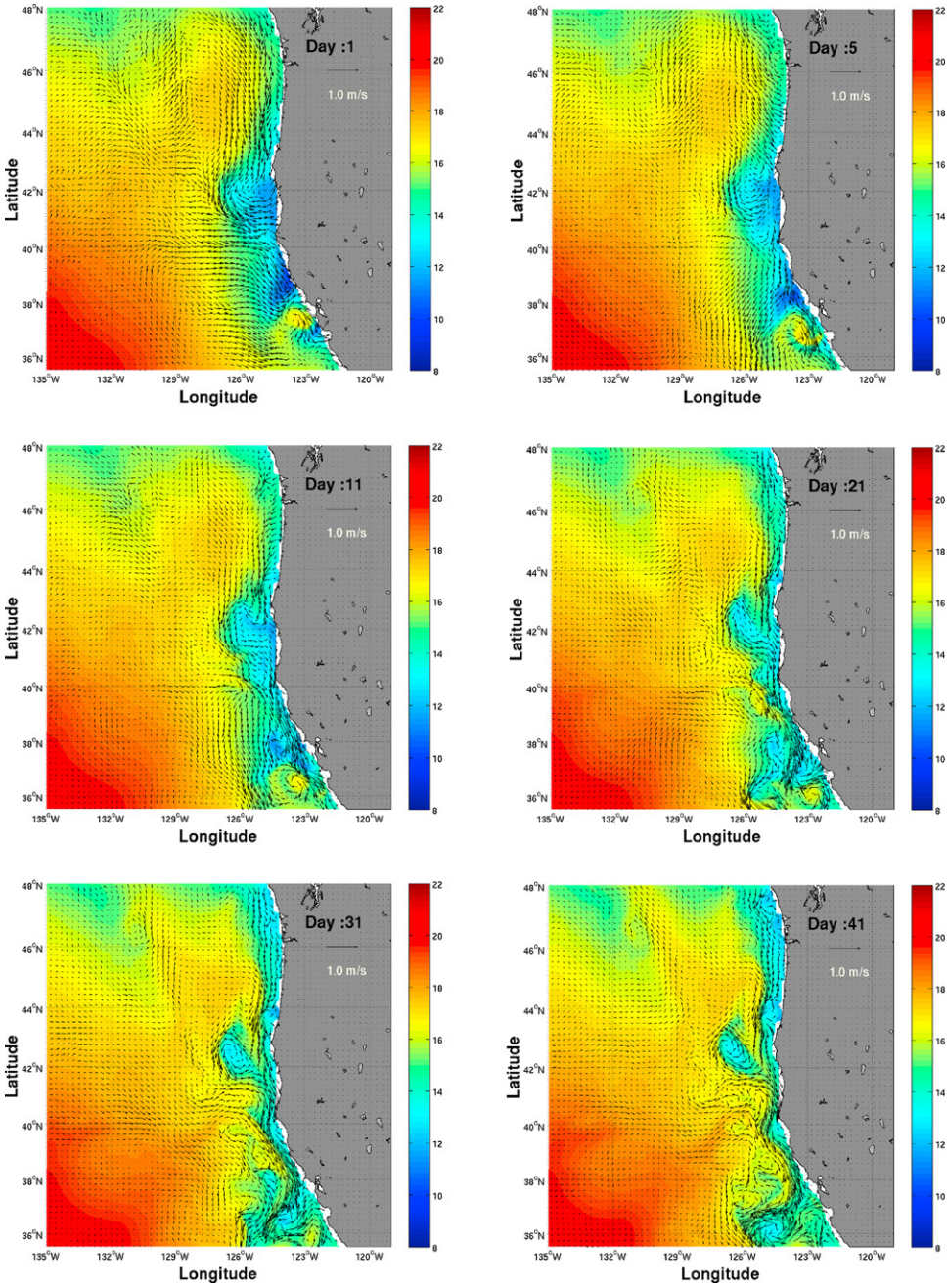


**Fig. 13.** Evolution of 40 days of surface temperature and velocity fields. See Section 6.1 for details on the evolution. Days 1, 5, 11, 21, 31 and 41 are referred as a, b, c, d, e and f in text.

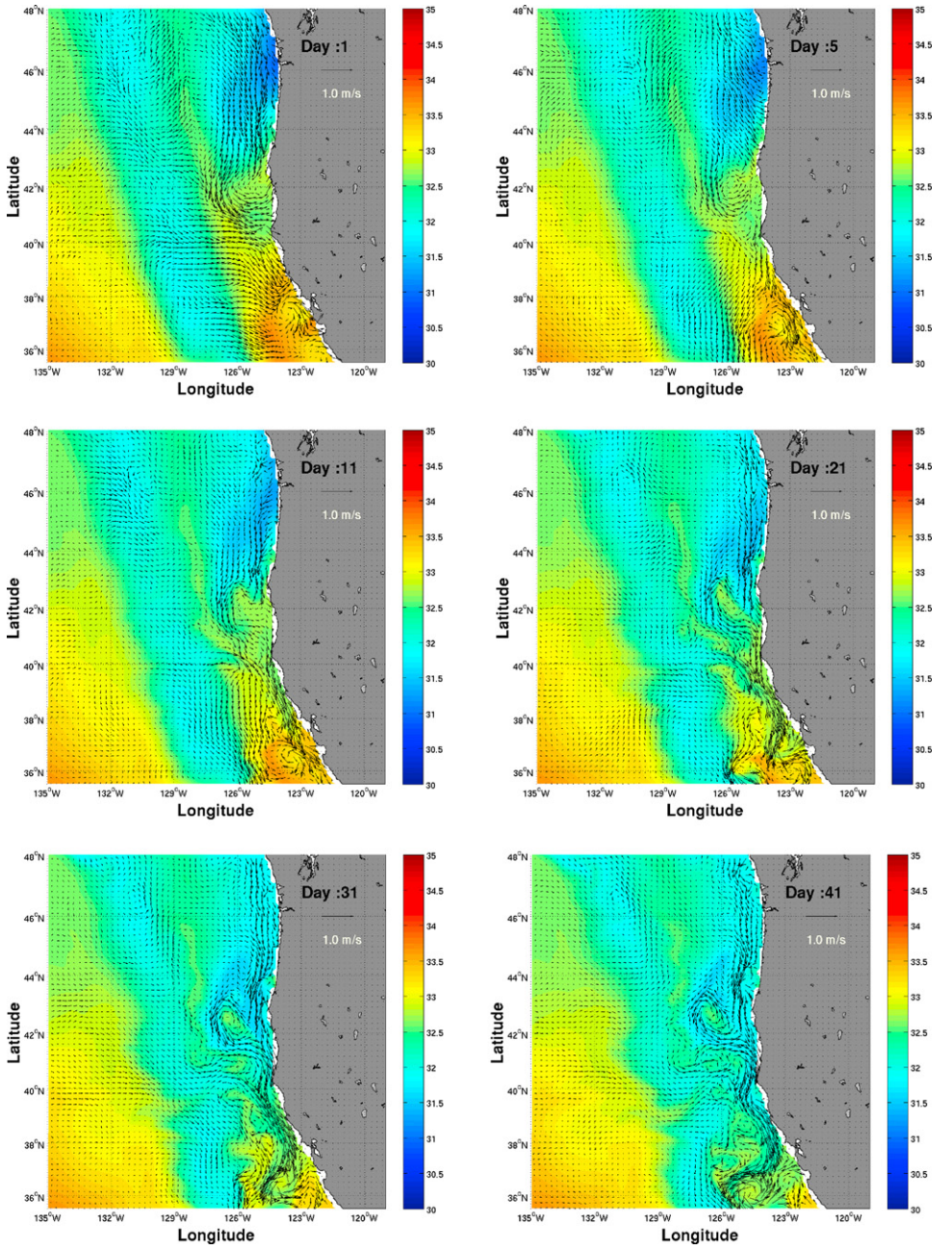


**Fig. 14.** Evolution of 40 days of surface salinity and velocity fields. Days 1, 5, 11, 21, 31 and 41 are referred as a, b, c, d, e and f in text.

both at the surface (Section 6.1) and at greater depths (Section 6.2). We then compare these results to those obtained from a classic climatological run with initial velocities in geostrophic balance with the climatological tracer fields (Section 6.3).

### 6.1. The surface temperature and salinity evolution

The evolution of the CCS-FORMS initialization for a typical summer synoptic realization is described here (Figs. 13 and 14). This simulation was run without any atmospheric forcing to study the internal adjustment and evolution of the FORMS-based initialization. The design of this initial field was based on 150 strategically sampled locations of the CC, CUC and upwelling FMs in a circulation template (Fig. 13) as explained in Section 5.1. Temperature fields (with current vectors overlaid) for days 1, 5, 11, 21, 31 and 41 are presented in six panels (Fig. 13). The initial field includes the upwelling around the capes and the southward-flowing current with the low-salinity pool (Fig. 14a) identified as the CC core. A continuous southward-flowing current develops along the coast by day 11. Additionally, a narrow region, similar to the CTZ, develops during the third week.

As mentioned in the previous section, the upwelling regions were included at initialization as FMs. Evidently, there are two mesoscale eddy developments at 42°N and at 38°N. Based on CTZ satellite and field data analyses during May–July 1987 and 1988 (Strub et al., 1991), a surface meandering jet surrounded by a field of eddies occurred between 36 and 42°N. Large dynamic height ranges corresponding to well-developed eddies were found. Eddies occurred mostly inshore of the jet north of 39°N, and were both inshore and offshore of the jet south of 39°N. In the present simulations, starting with the jet and upwelling regions in the FORMS setting, a large eddy inshore of the jet formed at around 42°N. A number of additional eddies (both cyclonic and anti-cyclonic) were also generated (Fig. 13d–f). On the larger scale, the dynamical evolution of the temperature field is similar to that of the synoptic SST field (Fig. 1a), indicative of the robustness of the model simulations.

The low-salinity core of the CCS is initialized (Fig. 14) as a jet FM and dynamically adjusts and evolves during the simulation while interacting with the surrounding waters. The high-salinity signature of the eddy development at 42°N is clearly seen within the spread of the low-salinity coastal waters. The boundary of the CTZ is probably best designated by the dynamic narrow band of high salinity between the low-salinity core of the CC and upwelling regions along the coast. The mesoscale eddy evolution at the surface during the first month of simulation is presented in terms of eddy kinetic energy (Fig. 15a–f). The evolution of this mesoscale field in a focused region near coast is examined (Fig. 16).

Several realistic features are observed during the 5–30 days of simulation (Fig. 16). First, an anticyclone off Monterey Bay is seen by day 5 at 37°N. This is accompanied by another adjacent small cyclone at 38°N. The cyclone continues to grow and maintain itself through day 30. The anticyclone off Monterey Bay interacts with the meandering jet, and a set of three adjacent anticyclonic-cyclonic-anticyclonic eddies (an ACE-CE-ACE triad) develops by day 20, which persists through day 30. In the northern part of the domain, a cyclone at 42–43°N, 126–127°W is apparent by day 10, and moves NW continuously through day 30. This eddy is originally connected with the upwelling at Cape Mendocino (41.5°N). A quick succession of cyclones and anticyclones occur near 40°N. The region near 40°N, 126°W is the most variable in the simulation.

The series of cyclones and anticyclones developed by day 20 (Fig. 16, bottom left) warrants further discussion. This evolution resembles the schematic in Fig. 2: the middle as well as the third panel indicates that the dynamical evolution of the CCS is a combination of the series of eddies and the jet-meander-eddy system. The simulated convergent shelf flow near Cape Mendocino has been observed (Magnell et al., 1990). An anticyclonic eddy similar to (albeit smaller than) the observed seasonally recurring giant eddy recently described by Crawford and Stone (2008) is simulated near 39°N, 125°W. There are distinct subsurface signatures of some of these surface eddies, which are described in the next subsection (Figs. 17–19).

A chlorophyll image (for September 2001) is compared with the model evolution on day 20 (Fig. 20). There are distinct resemblances in the eddy activity in a number of sub-regions between the inde-

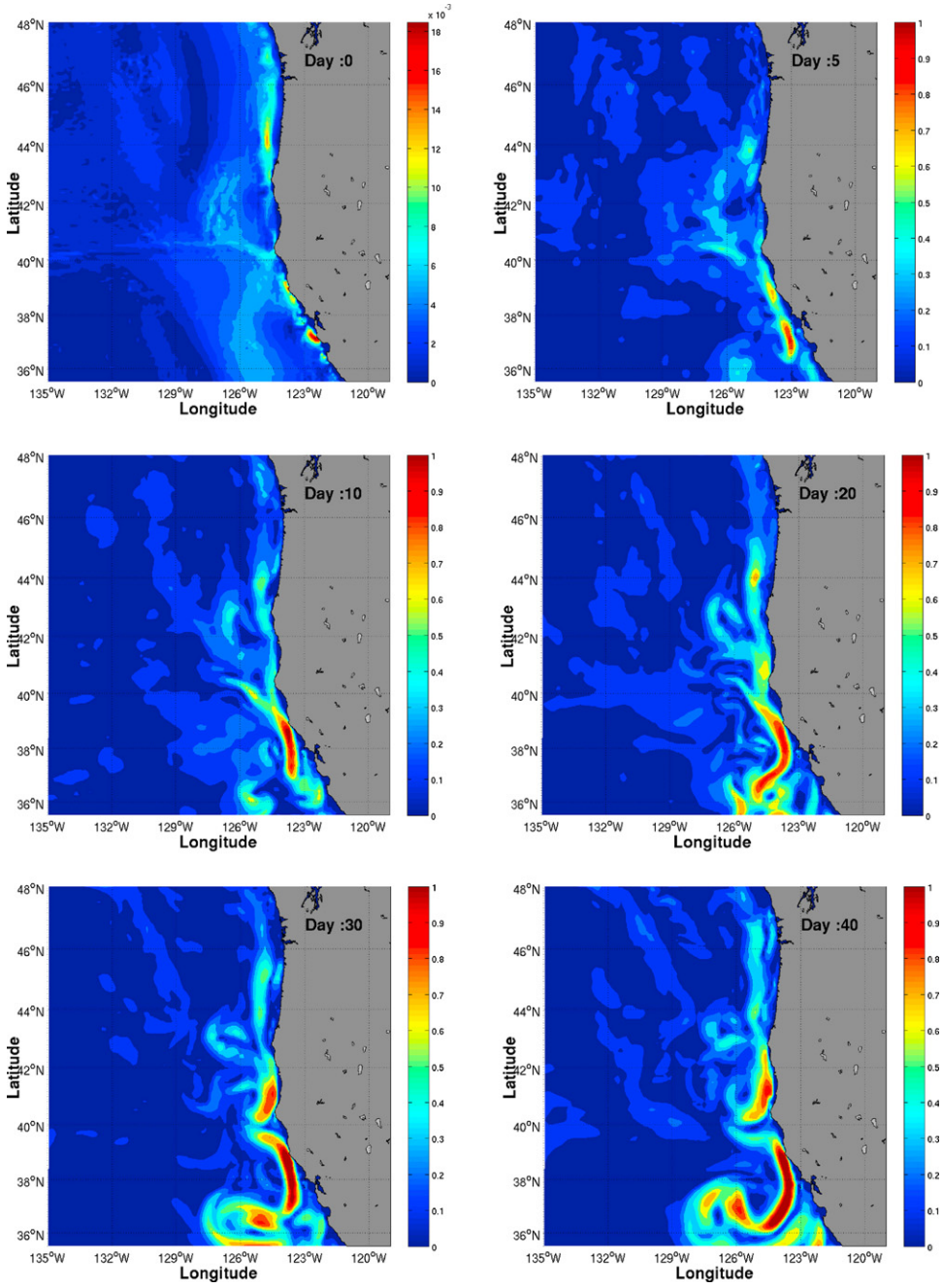


**Fig. 15.** Evolution of 40 days of eddy kinetic energy (kg m$^{-1}$ s$^{-2}$) at the surface. Days 0, 5, 10, 20, 30 and 40 are referred as a, b, c, d, e and f in text.

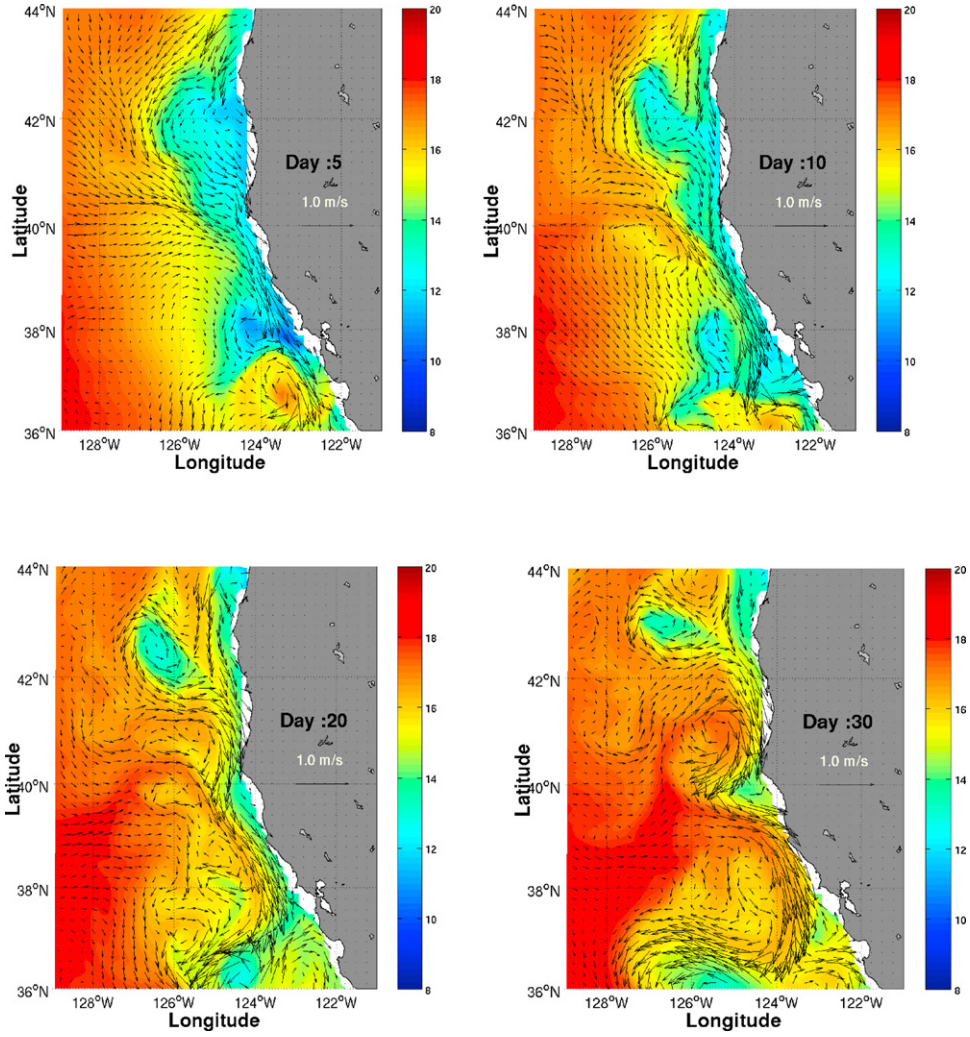


**Fig. 16.** Coastal zoom in the FORMS simulation, focusing on the region (36–44N, 129–121W), shows a month-long evolution of the mesoscale eddy field on the surface starting from the meander-upwelling FORMS-based initialization.

pendent image and the simulated temperature field which was evolved by POM starting from the feature-based initialization without any eddy field.

### 6.2. *Subsurface evolution (300 m and 1000 m)*

At 300 m, the known circulation of the CCS during summer is primarily eddy-driven, with significant subsurface eddies (Brink et al., 2000). The simulated evolution of the temperature, salinity, and velocity fields at 300 m are examined (Fig. 17). The subsurface eddies are visible in both temperature and salinity fields. Since the low-salinity pool of the CC core was feature-modeled to be restricted vertically to above 160 m, it does not penetrate to the intermediate depths. The subsurface signature of the surface eddies at 42°N and 38°N is apparent (Fig. 17a and b). Based on the

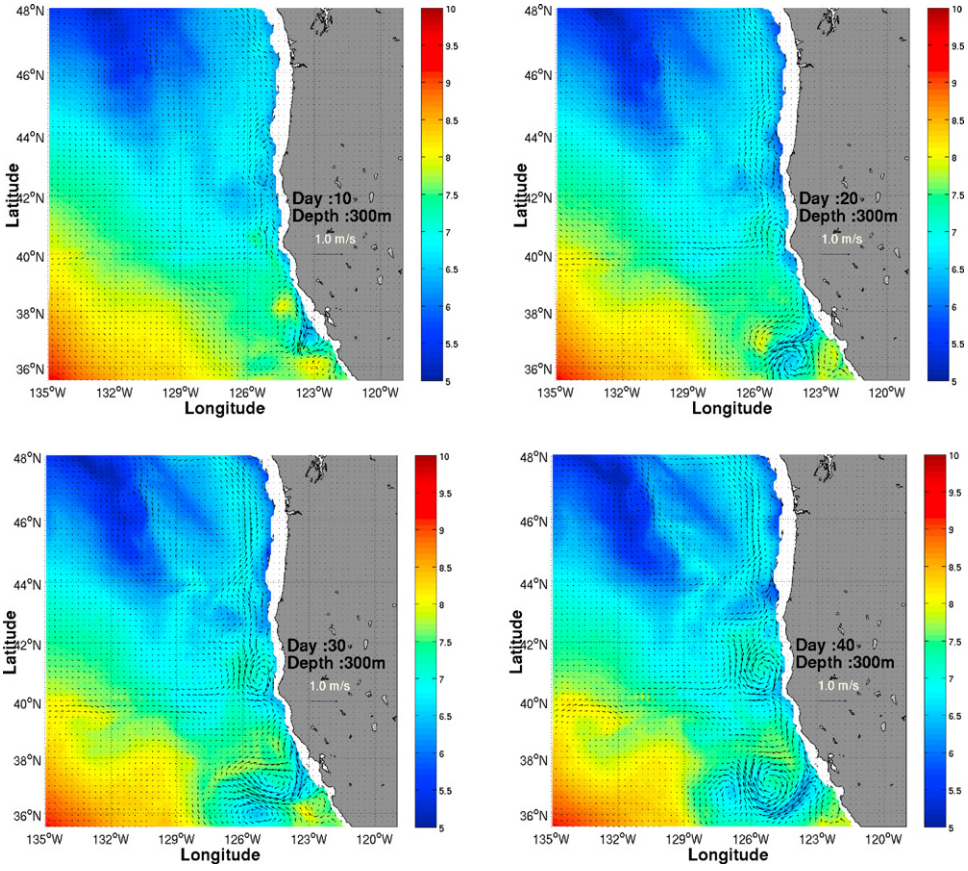


**Fig. 17.** Evolution of 40 days of temperature and velocity fields at 300 m. See Section 6.2 for details on the evolution. Days 10, 20, 30 and 40 are referred as a, b, c, and d in text.

mesoscale evolution near the coast inshore of 130°W during the first four weeks of the simulation (Fig. 18), the subsurface signature of the surface eddies at 36°N, forming the ACE-CE-ACE triad (Fig. 16), is evident on day 20. By day 30 this triad evolves into a CE-ACE pair similar to that at the surface.

From the 1000 m flow evolution (Fig. 19) for days 1, 5, 10, 20, 30 and 40, it is clear that, in addition to forming subsurface eddies, there is a natural tendency for poleward flow development along the California coast. Note that this coastal undercurrent is the natural pathway for the low-oxygen, nutrient-rich water which originates in the eastern tropical Pacific. Thus, the FORMS-CCS could be useful for predicting the biogeochemistry of the CCS in the future.

A series of anticyclonic eddies developed near the coast inshore of the poleward flow during the simulation. By day 5, an ACE develops first near the coast at 37°N. A poleward continuous flow develops at 1000 m by day 10. The ACE at 37°N grows between day 10 and day 40. By day 20, a second ACE is formed inshore of poleward flow near 40–41°N, and grows in size by day 30. A third inshore ACE develops at 44°N at around day 40. In addition to the ACEs, an ACE-CE pair occurred between 36 and 38°N (similar to the surface pair) on day 20. The smaller CE signature dissipated by day 30. The sizes and nature of the simulated eddies discussed above, along with some observational evidence of these eddies in past studies, is summarized in Table 5.

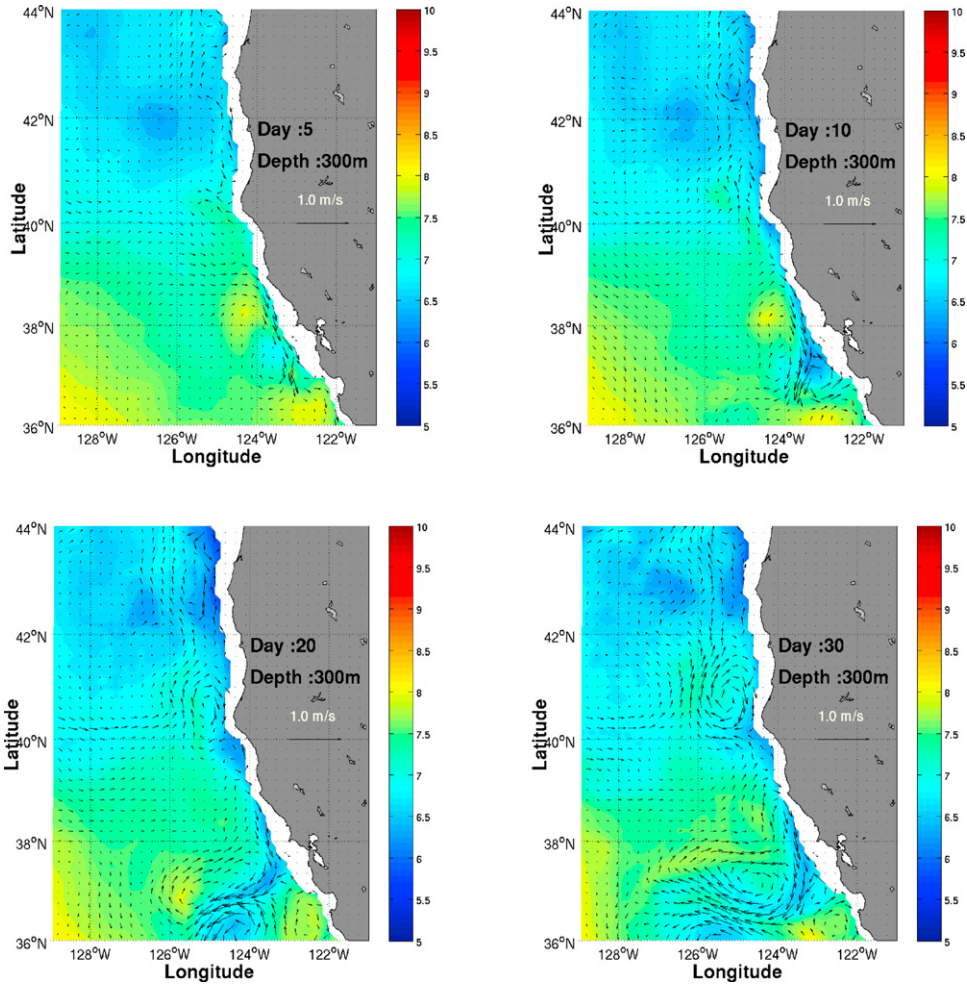


**Fig. 18.** Coastal zoom in the FORMS simulation, focusing on the region (36–44N, 129–121W), shows a month-long evolution of the mesoscale eddy field at 300 m starting from the meander-upwelling FORMS-based initialization.

### *6.3. A comparison with a climatology-only simulation*

Finally, a purely climatological simulation (Fig. 21) is compared with the FORMS simulation. This simulation was initialized with Levitus climatology (temperature and salinity) for August, without any FORMS components such as the CC, CUC or the upwelling FMs, and derived geostrophic velocity. Such velocity-inclusive initialization accelerates the spin-up and generally evolves mesoscale features faster (Calado et al., 2008; Lam et al., 2009; Haley and Lermusiaux, 2010; Lermusiaux et al., 2011). This climatology-initialized simulation, like its FORMS counterpart (Figs. 13–19), was carried out without any atmospheric forcing to study the internal dynamical evolution of the CCS.

Temperature, salinity, and EKE at the surface are examined along with temperature at 300 m and 1000 m on day 30 of the simulation (Fig. 21). At the surface, the FM evolution captures the mesoscales with higher amplitudes and linked with the upwelling regions; thus the finer-scale structures are more apparent in the FM simulation (compare Fig. 21a with Fig. 13e). The low-salinity pool is evident throughout the month-long FM simulation, and its existence allows for mesoscale eddies and finer-scale evolution within the coastal transition zone (compare Fig. 21b with Fig. 14e). In contrast, there is a

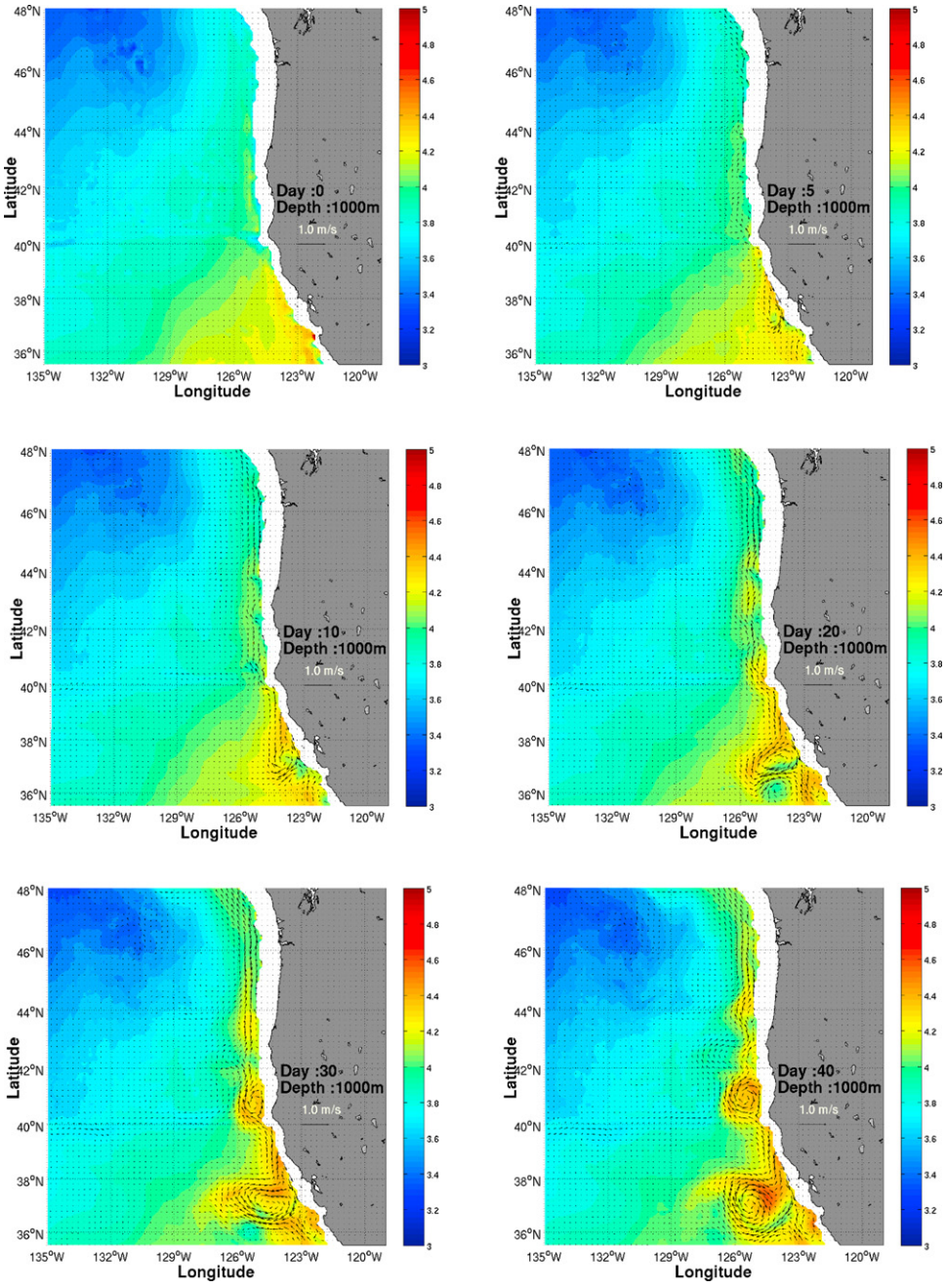


**Fig. 19.** Evolution of 40 days of temperature and velocity fields at 1000 m. See Section 5.3 for details on the evolution. Days 0, 5, 10, 20, 30 and 40 are referred as a, b, c, d, e and f in text.

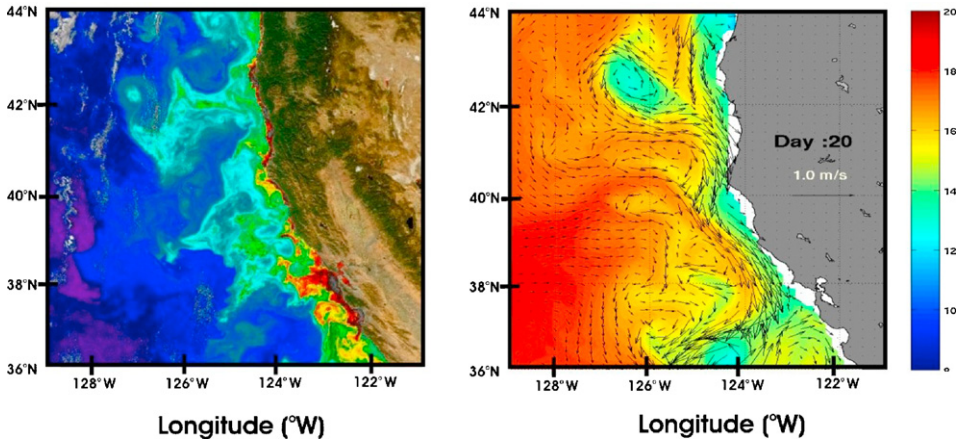


**Fig. 20.** A SeaWifs image from September 21, 2001 (left) shows eddy activity, which has some similarities to the model simulation on day 20. Note the resemblance in eddies at 42N, 40N and 36N. Furthermore, the complicated multiple eddies between 37 and 40N in the model is somewhat similar to the smaller eddies visible between 38 and 40N in the image on the left. (Image Courtesy of NASA/Goddard Space Flight Center, the SeaWiFS Project and GeoEye, Scientific Visualization Studio.)

tendency toward freshwater spreading offshore in the climatological simulation (Fig. 14e). This spread of lower salinity in the climatological simulation (day 30, Fig. 21b) is a slow progression following the southward surface flow (see Fig. 21c for a zoom on day 10). In contrast, the FORMS simulation (day 30, Fig. 14e) shows constrained progression and an eddy-dominated field. This contrast is due to the presence of the CUC and the upwelling FMs along the coast preventing the unrealistic spreading of low-salinity water of subarctic origin throughout most of the domain in the climatological simulation. In fact, the climatological simulation fails to initiate an energetic countercurrent (Fig. 21d and e). This can be a shortcoming even if advanced data assimilation schemes are used in simulations initiated with such climatological fields; if expected features are already in the initialization in some form, the potential for assimilation shocks is reduced.

A striking difference is the development of the equatorward-flowing narrow band of CC core current following the low-salinity pool, which is present in the FORMS simulation (Fig. 14) but absent from the

**Table 5**
Nature and characteristics of simulated vs. observed eddies in the CCS region (36–48N).

| Eddy type | Eddy Center | Size (simulated) | Size (observed) | Observational evidence (reference) | Comments |
|---|---|---|---|---|---|
| ACE1 | Pt. Sur | Radius ($R$) of 25–50 km | $R$ of 50–100 km | Ramp et al. (1997b) | Caused flow reversal down to 1000 m (>20 cm/s in 300 m; >30 cm/s at 100 m) |
| ACE2 | Pt. Arena | 50 km | $R$ of 50–100 km | Lagerloef (1992) | |
| CW-CCW pairs | Off Monterey Bay | >50 km | 50–100 km | Lagerloef, 1992 (Fig. 9) | |
| Cuddies | CUC Eddy | 25–35 km | | Cornuelle et al. (2000) | |
| Anticyclones | Cuddies | At different locations near Capes | $R$ < 35 km | Garfield et al. (1999, 2001) | Propagate westward at 1–2 cm/s |
| | Larger eddies at 300 m | $R$ > 25 km | $R$ > 50 km | Garfield et al. (1999, 2001) | |

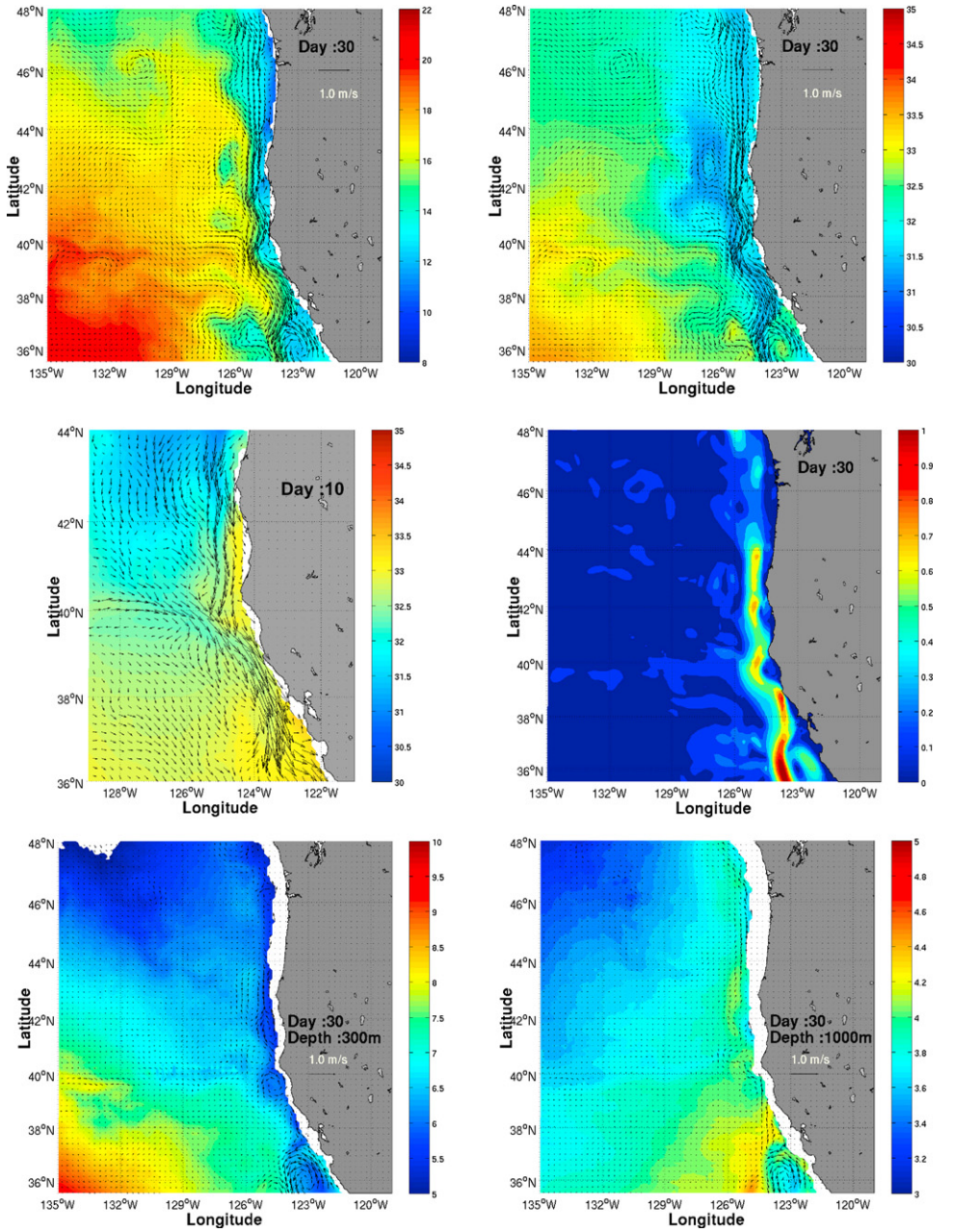


**Fig. 21.** Summary of evolution of the climatology simulation. Temperature (a) and salinity (b) are overlaid with velocity vectors on day 30; a coastal zoom focusing on 36–44N shows the salinity evolution on day 10 (c); surface EKE ($kg\,m^{-1}\,s^{-2}$) is shown on day 30 (d). Temperature fields overlaid with velocity for 300 m (d) and for 1000 m (e) are shown for day 30 of the simulation.

climatology-based simulation (Fig. 21a and b). The EKE structure for the climatological simulations is along a very narrow along-coast band (Fig. 21d), unlike the more realistic mesoscale-resolving distribution for the FM solution (Fig. 15e). The apparent wave-like pattern along 38°N and 40°N (Fig. 21a) in this simulation is a result of adjustment of the climatological fields to the underlying bathymetric ridge along these latitudes. This adjustment is visible in the initial EKE field of day 0 (Fig. 15a) and its subsequent development (Fig. 21d). The inclusion of the low-salinity pool CC core FM in the FORMS implementation modified and inhibited the growth of this wavy pattern; however, a hint of such growth is visible in the FORMS simulation during days 30 and 40 west of the low-salinity pool area (Figs. 13e and f).

The subsurface evolutions of the climatological simulations at 300 m and at 1000 m show little mesoscale activities and no development of cuddies (compare Fig. 21e with Fig. 17c and Fig. 21f with Fig. 19e). Clearly, the induction of the CUC in the FORMS methodology simulates the cuddies at the proper locations near capes (Cornuelle et al., 2000; Garfield et al., 1999, 2001) (Figs. 17–19, and Table 5). These comparisons indicate that, from a forecasting perspective, it might also be beneficial to assimilate data into a FORMS-initialized forecast rather than into a purely climatological initialization-based forecast or a spin-up climatology simulation.

## 7. Conclusions and discussion

This study developed and applied a feature-oriented regional modeling system (FORMS) for the CCS, including a prerequisite description of regional ocean features. The multiscale circulation features that are the characteristics of this eastern boundary current system include the mean flow and southeastward meandering jet(s) of the California Current, the poleward California Undercurrent, and six upwelling regions along the western coast of the U.S. (Fig. 3). The typical synoptic width, location, vertical extent, and core characteristics of these features were identified, and their dominant spatial and temporal scales of variability were summarized from past observational, theoretical and modeling studies (Table 1). These features were then melded with a climatology of the region for initialization of a primitive-equation modeling system, POM.

Dynamical simulations over a 40-day period using POM illustrate the applicability of FORMS to a transient eastern boundary current region such as the CCS. The simulations initialized with FORMS evolved various interactions among the low-salinity pool, the background climatology and the upwelling regions. A number of anticyclones and cyclones appeared at places where observational evidence of such eddies was documented in previous studies (Table 5). In addition, a countercurrent developed in the intermediate to deep waters along the coast, and shed realistic eddies ("cuddies") near a number of capes.

This phenomenological validation is the first step towards building a FORMS-based prediction system for this region. The immediate next step would be to statistically validate such simulations (initialized with low-salinity pool, coastal upwelling, CUC, CC, eddies and background climatology) following the works of Robinson and Gangopadhyay (1997) for the western North Atlantic. A number of hindcast studies using the summer experiments in Monterey Bay (ASON-II, MB06) and other historical datasets will need to be carried out to understand the parameter space behavior of the FMs. In addition, the FMs will have to be extended for other seasons and reevaluated for seasonal statistics before a truly operational system for the CCS-FORMS is implemented. Similar developments were completed for the Gulf of Maine (Brown et al., 2007a, b) before implementing the operational system for MARACOOS (Schmidt and Gangopadhyay, under review). Following Lozano et al. (1996), the FMs could now be used to augment the data utilized in advanced data-assimilative models such as those used by NCOM (Shulman et al., 2007, 2009), UCLA-ROMS (Marchesiello et al., 2003; Gruber et al., 2006; Capet et al., 2008a,b,c), JPL-ROMS (Li et al., 2008a,b), UCSC-ROMS (Veneziani et al., 2009a,b; Broquet et al., 2009; Goebel et al., 2010), Global NCOM (Barron et al., 2006), MSEAS (Haley and Lermusiaux, 2010), and others. For example, the FMs can be augmented with error fields which are based on prior knowledge of the range of variations of temperature and salinity of a particular feature at a particular time or season. New feature models can also be developed to initialize error covariance or ensembles for an assimilation scheme, extending the use of statistical-dynamical models (Lermusiaux, 2002) for uncertainty initialization to feature models.

As mentioned in the introduction, this development of FORMS for the CCS can now be useful for process-oriented dynamical studies to understand multiscale interactions between circulation features and climatology. In this first application of FORMS for an eastern boundary current region, a number of first-order analytical and empirical FMs were presented. The simulations initialized with FORMS showed surface and subsurface evolutions than were more realistic than evolutions in simulations initialized from climatology. In the future, more complex FMs will need to be developed for this region, including river inputs and wind forcing, and features such as CTWs, mushroom-like vortex pairs, filaments and squirts. Similar structures are also abundant in other oceanic regions such as the western North Atlantic, and such developments in a concerted effort are recommended.

## Acknowledgements

This work was funded by the Office of Naval Research grants N00014-03-1-0411 and N00014-03-1-0206 at the University of Massachusetts at Dartmouth. Leslie Rosenfeld's participation was supported by ONR grant N00014-03-WR-20009. PFJL, PJH and WGL are grateful to ONR for support under grant N00014-08-1-1097, N00014-08-1-0680 and MURI-ASAP to the Massachusetts Institute of Technology. Our special thanks to Dr. Jim Bellingham and his group at MBARI for numerous informative discussions and for making the data available from the MUSE and AOSN2 experiments. We are grateful to all who contributed to this effort by providing datasets. We especially acknowledge Drs. Ken Brink, Tommy Dickey, Francisco Chavez, Toby Garfield, Alex Warn-Varnas, Shaun Johnston, Curt Collins, Margaret McManus, Libe Washburn, and Erika McPhee-Shaw for their help and support in procuring the datasets from various sources. We also learned from discussions with Steve Ramp, Naomi Leonard, Russ Davis and Dave Fratantoni. We appreciate the editorial assistance provided by Mr. Frank Smith and graphics help of Ms. Carolina Nobre at SMAST. Finally, we are grateful to two anonymous reviewers for their insightful comments and encouragement for an earlier version of this manuscript, which led to substantial improvement of the presentation. We also thank Art Miller for his editing work and comments. This is an AOSN and MBO6 Contribution. This is number 11-0102 in the SMAST Contribution Series, School for Marine Science and Technology, University of Massachusetts Dartmouth.

## References

Abbott, M.R., Barksdale, B., 1991. Phytoplankton pigment patterns and wind forcing off central California. Journal of Geophysical Research 96, 14649–14667.

Abbott, M.R., Zion, P.M., 1987. Spatial and temporal variability of phytoplankton pigment off Northern California during CODE-1. Journal of Geophysical Research 92, 1745–1756.

Allen, J.S., Walstad, L.J., Newberger, P.A., 1991. Dynamics of the Coastal Transition Zone Jet. 2. Nonlinear finite amplitude behavior. Journal of Geophysical Research 96, 14995–15016.

Barron, C.N., Kara, A.B., Martin, P.J., Rhodes, R.C., Smedstad, L.F., 2006. Formulation, implementation and examination of vertical coordinate choices in the global Navy Coastal Ocean Model (NCOM). Ocean Modelling 11 (3–4), 347–375, doi:10.1016/j.ocemod. 2005.01.004.

Barth, J.A., Checkley, D.M., 2009. Patterns and processes in the California Current System. Progress in Oceanography 83, 49–64.

Barth, J.A., Pierce, S.D., Smith, R.L., 2000. A separating coastal upwelling jet at Cape Blanco, Oregon and its connection to the California Current System. Deep-Sea Research II 47, 783–810.

Barth, J.A., Pierce, S.D., Cowles, T.J., 2005. Mesoscale structure and its seasonal evolution in the northern California Current System. Deep-Sea Research II 52 (2005), 5–28.

Belkin, I.M., Cornillon, P.C., Sherman, K., 2009. Fronts in large marine ecosystems. Progress in Oceanography 81 (1–4), 223–236.

Bennett, A.F., 1992. Inverse Methods in Physical Oceanography. Cambridge University Press, Cambridge, 346 pp.

Bernstein, R.L., Breaker, L., Whitner, R., 1977. California Current eddy formation: ship, air and satellite results. Science 195, 353–359.

Blumberg, A.F., Kantha, L.H., 1985. Open boundary condition for circulation models. Journal of Hydraulics Engineering ASCE 111 (2), 237–255.

Blumberg, A.F., Mellor, G.L., 1987. A description of a three dimensional coastal ocean circulation model. In: Heaps, N.S. (Ed.), Three-dimensional Coastal Ocean Models. American Geophysical Union, Washington, pp. 1–16.

Boyer, T., Levitus, S., Garcia, H., Locarnini, R.A., Stephens, C., Antonov, J., 2005. Objective analyses of annual, seasonal, monthly temperature and salinity for the World Ocean on a 0.25° grid. International Journal of Climatology 25 (7), 931–945.

Brink, K.H., 1982. A comparison of long coastal trapped wave theory with observations off Peru. Journal of Physical Oceanography 12, 897–913.

Brink, K.H., Cowles, T.J., 1991. The coastal transition zone program. Journal of Geophysical Research 96, 14637–14647.

Brink, K.H., Beardsley, R.C., Niiler, P.P., Abbott, M., Huyer, A., Ramp, S., Stanton, T., Stuart, D., 1991. Statistical properties of near-surface flow in the California coastal transition zone. Journal of Geophysical Research 96, 14,693-14,706.

Brink, K.H., Beardsley, R.C., Paduan, J., Limeburner, R., Caruso, M., Sires, J.G., 2000. A view of the 1993–1994 California Current based on surface drifters, floats, remotely sensed data. Journal of Geophysical Research 105 (C4), 8575–8604.
Broquet, G., Edwards, C.A., Moore, A.M., Powell, B.S., Veneziani, M., Doyle, J.D., 2009. Application of 4D-Variational data assimilation to the California Current System, dynamics of atmosphere. Oceans, doi:10.1016/j.dynatmoce.2009.03.001.
Brown, W.S., Gangopadhyay, A., Bub, F.L., Yu, Z., Strout, G., Robinson, A.R., 2007a. An operational circulation modeling system for the Gulf of Maine/Georges bank region. Part 1. The basic elements. IEEE Journal of Oceanic Engineering 32 (4), 807–822.
Brown, W.S., Gangopadhyay, A., Yu, Z., 2007b. An operational circulation modeling system for the Gulf of Maine/Georges bank region. Part 2. Applications. IEEE Journal of Oceanic Engineering 32 (4), 807–822.
Bucklin, A., 1991. Population genetic responses of the planktonic copepod Metridia Pacifica to a coastal eddy in the California Current. Journal of Geophysical Research 96, 14799–14808.
Calado, L., Gangopadhyay, A., da Silveira, I.C.A., 2006. A parametric model for the Brazil Current meanders and eddies off southeastern Brazil. Geophysical Research Letters 33, L12602, doi:10.1029/2006GL026092.
Calado, L., Gangopadhyay, A., da Silveira, I.C.A., 2008. Feature-oriented regional modeling and simulations (FORMS) for the Western South Atlantic, Southeastern Brazil region. Ocean Modeling 25, 48–64.
Capet, X., McWilliams, J.C., Molemaker, M.J., Shchepetkin, A.F., 2008a. Mesoscale to submesoscale transition in the California Current System. Part I. Flow structure, eddy flux, observational tests. Journal of Physical Oceanography 38, 29–43.
Capet, X., McWilliams, J.C., Molemaker, M.J., Shchepetkin, A.F., 2008b. Mesoscale to submesoscale transition in the California Current System. Part II. Frontal processes. Journal of Physical Oceanography 38, 44–64.
Capet, X., McWilliams, J.C., Molemaker, M.J., Shchepetkin, A., 2008c. Mesoscale to submesoscale transition in the California Current System. III. Energy balance and flux. Journal of Physical Oceanography 38, 2256–2269.
Carriere, O., Hermand, J.P., Calado, L., Paula, A.C., Silveira, I.C.A., 2010. Range-dependent acoustic tomography based on a feature model for monitoring the Cabo Frio upwelling (Brazil). In: Sydney Conference—Showcasing Advances in Marine Science and Engineering, 2010, Sydney. Proceedings of OCEANS 10 IEEE, 2010.
Castelao, R.M., Campos, E.J.D., Miller, J.L., 2004. A modelling study of coastal upwelling driven by wind and meanders of the Brazil current. Journal of Coastal Research (July), 662–671.
Chao, Y., Li, Z., Farrara, J., McWilliams, J.C., Bellingham, J., Capet, X., Chavez, F., Choi, J.-K., Davis, R., Doyle, J., Fratantoni, D., Li, P., Marchesiello, P., Moline, M.A., Paduan, J., Ramp, S., 2009. Development, implementation, evaluation of a data-assimilative ocean forecasting system off the central California coast. Deep-Sea Research II, doi:10.1016/j.dsr2.2008.08.011.
Chavez, F.P., Collins, C.A. (Eds.), 2000a. Studies of the California Current System Part 2, vol. 47. Deep-Sea Research II, pp. 5–6.
Chavez, F.P., Collins, C.A., 2000b. Studies of the California Current System: present, past and future. Deep-Sea Research II 47, 761–763.
Chavez, F.P., Barber, R.T., Kosro, P.M., Huyer, A., Ramp, S.R., Stanton, T.P., Rojas de Mendiola, B., 1991. Horizontal transport and the distribution of nutrients in the coastal transition zone off northern California: effects on primary production, phytoplankton biomass and species composition. Journal of Geophysical Research 96, 14833–14848.
Chavez, F.P, Pennington, T.J., Herlien, R., Jannasch, H.W., Thurmond, G., Friederich, G., 1997. Moorings and drifters for real-time interdisciplinary oceanography. Journal of Atmospheric and Oceanic Technology 14, 1199–1211.
Chelton, D.B., 1984. Seasonal variability of alongshore geostrophic velocity off central California. Journal of Geophysical Research 89, 3473–3486.
Chelton, D., Schlax, M., 1991. Estimation of time averages from irregularly spaced observations: with application to Coastal Zone Color Scanner estimates of chlorophyll concentration. Journal of Geophysical Research 96, 14669–14692.
Chereskin, T.K., Niiler, P.P., 1994. Circulation in the Ensenada Front—September 1988. Deep-Sea Research Part I: Oceanographic Research Papers 41, 1251–1287.
Collins, C.A., Castro, C.G., Asanuma, H., Rago, T.A., Han, H.-K., Durazo, R., Chavez, F.P., 2002. Changes in the hydrography of Central California waters associated with the 1997–98 El Niño. Progress in Oceanography 54, 184–204.
Collins, C.A., Garfield, N., Paquette, R.G., Carter, E., 1996. Lagrangian measurement of subsurface poleward flow between 380°N and 430°N along the West Coast of the United States during Summer, 1993. Geophysical Research Letters 23 (September (18)), 2461–2464.
Collins, C.A., Garfield, N., Rago, T.A., Rischmiller, F.W., Carter, E., 2000. Mean structure of the inshore countercurrent and California undercurrent off point Sur, California. Deep-Sea Research II 47, 765–782.
Collins, C.A., Pennington, J.T., Castro, C.G., Rago, T.A., Chavez, F.P., 2003. The California Current System off Monterey, California: physical and biological coupling. Deep-Sea Research II 50, 2389–2404.
Cornuelle, B.D., Chereskin, T.K., Niiler, P.P., Morris, M.Y., Musgrave, D.L., 2000. Observations and modeling of a CA, undercurrent eddy. Journal of Geophysical Research C 105, 1227–1243.
Crawford, G., Stone, S., 2008. COCMP surface current mapping reveals eddy and upwelling jet off Cape Mendocino. In: American Geophysical Union, Fall Meeting 2008, Abstract #OS41B-1216.
Cummings, J.A., Szczechowski, C., Carnes, M.R., 1997. Global and regional ocean thermal analysis systems. Marine Technology Society Journal 31, 63–75.
Davis, R.E., 1985. Drifter observations of coastal surface currents during CODE: the method and descriptive view. Journal of Geophysical Research 90, 4741–4755.
Dewey, R.K., Moum, J.N., Paulson, C.A., Caldwell, D.R., Pierce, S.D., 1991. Structure and dynamics of a coastal filament. Journal of Geophysical Research 96, 14885–14907.
Di Lorenzo, E., Miller, A.J., Schneider, N., McWilliams, J.C., 2005. The warming of the California Current: dynamics and ecosystem implications. Journal of Physical Oceanography 35, 336–362.
Ezer, T., Mellor, G.L., 1994. Diagnostic ands prognostic calculations of the North Atlantic circulation and sea level using a sigma coordinate ocean model. Journal of Geophysical Research 99, 14159–14171.
Ezer, T., Mellor, G.L., 1997. Data assimilation experiments in the Gulf Stream region: how useful are satellite-derived surface data for nowcasting the subsurface fields? Journal of Atmospheric and Oceanic Technology 16 (6), 1379–1391.
Flament, P., Armi, L., Washburn, L., 1985. The evolving structure of an upwelling filament. Journal of Geophysical Research 90, 1765–1985.

Fox, D.N., Carnes, M.R., Mitchell, J.L., 1992. Characterizing Major Frontal Systems: a nowcast/forecast system for Northwest Atlantic. Oceanography 5, 49–53.
Fratantoni, D.M., Haddock, S.H.D., 2009. Introduction to the Autonomous Ocean Sampling Network (AOSN) program. Deep-Sea Research II 56, 61.
Gangopadhyay, A., Robinson, A.R., 2002. Feature-oriented regional modeling of oceanic fronts. Dynamics of Atmospheres and Oceans 36, 201–232.
Gangopadhyay, A., Robinson, A.R., Arango, H.G., 1997. Circulation and dynamics of the Western North Atlantic. I: Multi-scale feature models. Journal of Atmospheric and Oceanic Technology 14 (6), 1314–1332.
Gangopadhyay, A., Robinson, A.R., Haley Jr., P.J., Leslie, W.G., Lozano, C.J., Bisagni, J.J., Yu, Z., 2003. Feature oriented regional modeling and simulations (FORMS) in the Gulf of Maine and Georges Bank. Continental Shelf Research 23 (3–4), 317–353.
Gangopadhyay, A., Shen, C.Y., Marmorino, G.O., Mied, R.P., Lindemann, G., 2005. An Extended Velocity Projection method for estimating the subsurface current and density structure for coastal plume regions: an application to the Chesapeake Bay Outflow Plume. Continental Shelf Research 25, 1309–1319.
Garfield, N., Collins, C.A., Paquette, R.G., Carter, E., 1999. Lagrangian exploration of the California undercurrent, 1992–1995. Journal of Physical Oceanography 29, 560–583.
Garfield, N., Maltrud, M.E., Collins, C.A., Rago, T.A., Paquette, R.G., 2001. Lagrangian flow in the California undercurrent, an observation and model comparison. Journal of Marine Systems 29 (1–4), 201–220.
Glenn, S.M., Robinson, A.R., 1995. Validation of an operational Gulf Stream forecasting model, qualitative skill assessment for coastal models. AGU Estuarine/Coastal Series, vol. 47. American Geophysical Union, pp. 469–499.
Goebel, N., Edwards, C.A., Zehr, J., Follows, M., 2010. Resolving phytoplankton biodiversity in an ecosystem model within the California Current System. In: Proceedings from the 2010 AGU Ocean Sciences Meeting , 22–26 February, 2010.
Graf, J., Sasaki, C., Winn, C., Liu, W.T., Tsai, W., Freilich, M., Long, D., 1998. NASA scatterometer experiment. Acta Astronautica 43, 397–407.
Gruber, N., Frenzel, H., Doney, S.C., Marchesiello, P., McWilliams, J.C., Moisan, J.R., Oram, J.J., Plattner, G.K., Stolzenbach, K.D., 2006. Eddy-resolving simulation of plankton ecosystem dynamics in the California Current System. Deep Sea Research I 53, 1483–1516.
Haidvogel, D.U., Beckmann, A., Hedstrom, K.S., 1991. Dynamical simulations of filament formation and evolution in the Coastal Transition Zone. Journal of Geophysical Research 96, 15017–15040.
Haley Jr., P.J., Lermusiaux, P.F.J., 2010. Multiscale two-way embedding schemes for free-surface primitive-equations in the multidisciplinary simulation, estimation and assimilation system. Ocean Dynamics 60, 1497–1537, doi:10.1007/s10236-010-0349-4.
Haley Jr., P.J., Lermusiaux, P.F.J., Robinson, A.R., Leslie, W.G., Logoutov, O., Cossarini, G., Liang, X.S., Moreno, P., Ramp, S.R., Doyle, J., Bellingham, J.G., Chavez, F.P., Johnston, S., 2009. Forecasting and reanalysis in the Monterey Bay/California current region for the Autonomous Ocean Sampling Network-II experiment. Deep-Sea Research II 56, 127–148.
Hasegawa, D., Lewis, M., Gangopadhyay, A., 2009. How islands cause phytoplankton to bloom in their wakes. Geophysical Research Letters 36, L20605, doi:10.1029/2009GL039743.
Haynes, R., Barton, E.D., 1991. Lagrangian observations in the Iberian coastal transition zone. Journal of Geophysical Research 96, 14731–14742.
Hayward, T.L., Mantyla, A.W., 1990. Physical, chemical and biological structure of a coastal eddy near Cape Mendocino. Journal of Marine Research 4, 825–850.
Heathershaw, A.D, Foreman, S.J., 1996. FOAM—a forecasting ocean–atmosphere model for naval applications. Journal of Defence Science 1, 434–438.
Hickey, B.M., 1998. Coastal oceanography of Western North America from the tip of Baja California to Vancouver Is. In: Brink, K.H., Robinson, A.R. (Eds.), The Sea, vol. 11. Wiley and Sons, Inc., pp. 345–393 (Chapter 12).
Hulburt, H.E., Fox, D.N., Metzger, E.J., 1990. Statistical inference of weakly correlated subthermocline fields from satellite altimeter data. Journal of Geophysical Research 95, 11375–11409.
Hurlburt, H.E., Wallcraft, A.J., Schmitz Jr., W.J., Hogan, P.J., Metzger, E.J., 1996. Dynamics of the Kuroshio/Oyashio current system using eddy-resolving models of the North Pacific Ocean. Journal of Geophysical Research 101, 941–976.
Huyer, A.E., 1983. Coastal upwelling in the California Current System. Progress in Oceanography 12, 259–284.
Huyer, A., Barth, J.A., Kosro, P.M., Shearman, R.K., Smith, R.L., 1998. Upper-ocean water mass characteristics of the California Current, summer 1993. Deep-Sea Research II 45, 1411–1442.
Huyer, A, Kosro, P.M., Fleischbein, J., Ramp, S.R., Stanton, T., Washburn, L., Chavez, F.P., Cowles, T.J., Pierce, S.D., Smith, R.L., 1991. Currents and water masses of the Coastal Transition Zone off northern California, June to August, 1988. Journal of Geophysical Research 96, 14809–14831.
Huyer, A., Kosro, P.M., Lentz, S., Beardsley, R.C., 1989. Poleward flow in the California Current System. In: Neshyba, S.J., Mooers, C.N.K., Smith, R.L., Barber, R.T. (Eds.), Poleward Flows Along Eastern Ocean Boundaries. Coastal and Estuarine Studies, vol. 34. Springer-Verlag, pp. 142–156.
Ikeda, M., Emery, W.J., 1984. Satellite observations and modeling of meanders in the California Current System off Oregon and Northern California. Journal of Physical Oceanography 14, 1434–1450.
Johns, T.C., Carnel, R.E., Crossley, J.F., Gregory, J.M., Mitchell, J.F.B., Senior, C.A., Tett, S.F.B., Wood, R.A., 1997. The second Hadley centre coupled ocean–atmosphere GCM: model description, spinup and validation. Climate Dynamics 13, 103–134.
Kadko, D.C, Washburn, L., Jones, B., 1991. Evidence of subduction within cold filaments of the northern California coastal transition zone. Journal of Geophysical Research 96, 14909–14926.
Kelly, K.A., Beardsley, R.C., Limeburner, R., Brink, K.H., Paduan, J.D., Chereskin, T.K., 1998. Variability of the near-surface eddy kinetic energy in the California Current based on altimetric, drifter, moored current data. Journal of Geophysical Research 103 (C6), 13067–13083, doi:10.1029/97JC03760.
Kim, H.-S, Gangopadhyay, A., Rosenfeld, L.K., Bub, F.L., 2007. A high-resolution regional climatology for the Central California. Continental Shelf Research, doi:10.1016/j.csr. 2007.05.011.

Kosro, P.M., Huyer, A., Ramp, S.R., Smith, R.L., Chavez, F.P., Cowles, T.L., Abbott, M.R., Strub, P.T., Barber, R.T., Jessen, P., Small, L.F., 1991. The structure of the transition zone between coastal waters and the open ocean off northern California, winter and spring 1987. Journal of Geophysical Research 96, 14707–14730.

Lagerloef, G.S.E, 1992. The Point Arena Eddy: a recurring summer anticyclone in the California Current. Journal of Geophysical Research 97 (C8), 12557–12568.

Largier, J.L., Lawrence, C.A., Roughan, M., Kaplan, D.M., Dever, E.P., Dorman, C.E., Kudela, R.M., Bollens, S.M., Wilkerson, F.P., Dugdale, R.C., Botsford, L.W., Garfield, N., Kuebel-Cervantes, B., Koracin, D., 2006. WEST: a northern California study of the role of wind-driven transport in the productivity of coastal plankton communities. Deep Sea Research II 53 (25–26), 2833–2849.

Lam, F.P., Haley, P.J. Jr., Janmaat, J., Lermusiaux, P.F.J., Leslie, W.G., Schouten, M.W., te Raa, L.A., Rixen, M., 2009. At-sea Real-time Coupled Four-dimensional Oceanographic and Acoustic Forecasts during Battlespace Preparation 2007. Special issue of the Journal of Marine Systems on "Coastal processes: Challenges for Monitoring and Prediction", J.W. Book, M. Orlic, M. Rixen (Guest Eds.), 78, S306–S320, doi:10.1016/j.jmarsys.2009.01.029.

Lermusiaux, P.F.J., 1999a. Data assimilation via error subspace statistical estimation. Part II. Mid-Atlantic bight shelfbreak front simulations and ESSE validation. Monthly Weather Review 127 (8), 1408–1432.

Lermusiaux, P.F.J., 1999b. Estimation and study of mesoscale variability in the strait of Sicily. Dynamics of Atmospheres and Oceans 29, 255–303.

Lermusiaux, P.F.J., 2002. On the mapping of multivariate geophysical fields: sensitivity to size, scales and dynamics. Journal of Atmospheric and Oceanic Technology 19, 1602–1637.

Lermusiaux, P.F.J., 2006. Uncertainty estimation and prediction for interdisciplinary ocean dynamics. Special issue on "Uncertainty Quantification". J. Glimm and G. Karniadakis, Eds. Journal of Computational Physics, 176–199.

Lermusiaux, P.F.J., Anderson, D.G.M., Lozano, C.J., 2000. On the mapping of multivariate geophysical fields: Error and variability subspace estimates. Quarterly Journal of Royal Meteorological Society 126, 1387–1429.

Lermusiaux, P.F.J., Haley Jr., P.J., Leslie, W.G., Agarwal, A., Logutov, O., Burton, L.J., 2011. Multiscale physical and biological dynamics in the Philippines Archipelago: predictions and processes. Oceanography 24 (1), 70–89, doi:10.5670/oceanog.2011.05, Special PhilEx Issue.

Li, Z., Chao, Y., McWilliams, J.C., Ide, K., 2008a. A three-dimensional variational data assimilation scheme for the Regional Ocean Modeling System. Journal of Atmospheric and Oceanic Technology 25, 2074–2090, doi:10.1175/2008JTECHO594.1.

Li, Z., Chao, Y., McWilliams, J.C., Ide, K., 2008b. A three-dimensional variational data assimilation scheme for the Regional Ocean Modeling System: implementation and basic experiments. Journal of Geophysical Research 113, C05002, doi:10.1029/2006JC004042.

Lozano, C.J., Robinson, A.R., Arango, H.G., Gangopadhyay, A., Sloan, N.Q., Haley, P.J., Anderson, L., Leslie, W.G., 1996. An interdisciplinary ocean prediction system: assimilation strategies and structured data models. In: Mallanotte-Rizzoli, P. (Ed.), Modern Approaches to Data Assimilation on Ocean Modeling, vol. 61. Elsevier Oceanography Series, Amsterdam, pp. 413–452.

Lynn, R.J., Bliss, K.A., Eber, L.E., 1982. Vertical and horizontal distributions of seasonal mean temperature, salinity, sigma-t, stability, dynamic height, oxygen, oxygen saturation in the California Current, 1950–1978. In: CalCOFI Atlas No. 30. Scripps Institution of Oceanography, La Jolla, p. 513.

Lynn, R.J., Simpson, J.J., 1987. The California Current System: the seasonal variability of its physical characteristics. Journal of Geophysical Research 92, 12947–12966.

Mackas, D.L., Washburn, L., Smith, S.L., 1991. Zooplankton community pattern associated with a California Current cold filament. Journal of Geophysical Research 96, 14781–14797.

Magnell, B.A., Bray, N.A., Winant, C.D., Greengrove, C.L., Largier, J., Borchard, J.F., Bernstein, R.L., Dorman, C.E., 1990. Convergent shelf flow at Cape Mendocino. Oceanography 3 (1), 4–11.

Marchesiello, P., McWilliams, J.C., Shchepetkin, A., 2003. Equilibrium structure and dynamics of the California Current System. Journal of Physical Oceanography 33, 753–783.

Mathew, E.M., McClean, J.L., 2005. An eddy resolving global 1/10° ocean simulation. Ocean Modelling 8, 31–54.

McWilliams, J.C., 1985. Submesoscale, coherent vortices in the ocean. Review of Geophysics 23, 165–182.

Mied, R.P, 1990. Mushroom-like patterns of the ocean surface, Eos, transactions. American Geophysical Union 71 (49), 1837.

Mied, R.P., McWilliams, J.C., Lindemann, G.J., 1991. The generation and evolution of mushroom-like vortices. Journal of Physical Oceanography 21, 490–510.

Miller, A.J., 1996. Recent advances in California Current modeling: decadal and interannual thermocline variations. California Cooperative Oceanic Fisheries Investigations Reports 37, 69–79.

Miller, A.J., Di Lorenzo, E., Neilson, D.J., Cornuelle, B.D., Moisan, J.R., 2000. Modeling CalCOFI observations during El Niño: fitting physics and biology. California Cooperative Oceanic Fisheries Investigations Reports 41, 87–97.

Miller, A.J., McWilliams, J.C., Schneider, N., Allen, J.S., Barth, J.A., Beardsley, R.C., Chavez, F.P., Chereskin, T.K., Edwards, C.A., Haney, R.L., Kelly, K.A., Kindle, J.C., Ly, L.N., Moisan, J.R., Noble, M.A., Niiler, P.P., Oey, L.Y., Schwing, F.B., Shearman, R.K., Swenson, M.S., 1999. Observing and modeling the California Current System, Eos, transactions. American Geophysical Union 80, 533–539.

Moore, A.M., Arango, H.G., Di Lorenzo, E., Miller, A.J., Cornuelle, B.D., 2009. An adjoint sensitivity analysis of the Southern California current circulation and ecosystem. Journal of Physical Oceanography 39, 702–720.

Mooers, C.N.K., Robinson, A.R., 1984. Turbulent jets and eddies in the California current and inferred cross-shore transports. Science 223, 51–53.

Munk, W., Armi, L., Fischer, K., Zachariasen, F., 2000. Spirals on the sea. Proceedings of the Royal Society of London 456, 1217–1280.

Noble, M., Ramp, S.R., 2000. Subtidal currents over the central California slope: evidence for offshore veering of the undercurrent and for direct, wind-driven slope currents. Deep-Sea Research II 47, 871–906.

Oey, L., 1999. A forcing mechanism for the poleward flow off the southern California coast. Journal of Geophysical Research, 539, 104, 13,529-13.

Palma, E.D., Matano, R.P., 1998. On the implementation of passive open boundary conditions for a general circulation model: the barotropic mode. Journal of Geophysical Research 103, 1319–1341.

Penven, P., Debre, L., Marchesiello, P., McWilliams, J.C., 2006. Evaluation and application of the ROMS 1-way embedding procedure to the central California upwelling system. Ocean Modelling 12 (1–2), 157–187.
Pickett, M.H., Paduan, J.D., 2003. Ekman transport and pumping in the California Current based on the U.S. Navy's high resolution atmospheric model (COAMPS). Journal of Geophysical Research 108 (C10), 3327, doi:10.1029/2003JC001902.
Pierce, S.D., Smith, R.L., Kosro, P.M., Barth, J.A., Wilson, C.D., 2000. Continuity of the poleward undercurrent along the eastern boundary of the mid-latitude Pacific. Deep Sea Research 47, 811–829.
Pringle, J.M., Dever, E.P., 2009. Dynamics of wind-driven upwelling and relaxation between Monterey Bay and Point Arena: local-, regional-, gyre-scale controls. Journal of Geophysical Research 114, C07003, doi:10.1029/2008JC005016.
Ramp, S.R., Davis, R.E., Leonard, N.E., Shulman, I., Chao, Y., Robinson, A.R., Marsden, J., Lermusiaux, P.F.J., Fratantoni, D., Paduan, J.D., Chavez, F.P., Bahr, F.L., Liang, S., Leslie, W., Li, Z., 2009. Preparing to predict: the second Autonomous Ocean Sampling Network (AOSN-II) experiment in the Monterey Bay. Deep-Sea Research II, doi:10.1016/j.dsr2.2008.08.013.
Ramp, S.R., Jessen, P.F., Brink, K.H., Niiler, P.P., Daggett, F.L., Best, J.S., 1991. The physical structure of cold filaments near Point Arena, California, During June 1987. Journal of Geophysical Research 96, 14859–14883.
Ramp, S.R., Lermusiaux, P.F.J., Shulman, I., Chao, Y., Wolf, R.E., Bahr, F.L., this issue. Oceanographic and atmospheric conditions on the continental shelf north of the Monterey Bay during August 2006. Dynamics of Atmosphere and Oceans.
Ramp, S.R., McClean, J.L., Collins, C.A., Semtner, A.J., Hays, K.A.S., 1997a. Observations and modeling of the 1991–1992 El Nino signal off central California. Journal of Geophysical Research 102, 5553–5582.
Ramp, S.R., Paduan, J.D., Shulman, I., Kindle, J., Bahr, F.L., Chavez, F.P., 2005. Observations of upwelling and relaxation events in the northern Monterey Bay during August 2000. Journal of Geophysical Research 110, C07013, doi:10.1029/2004JC002538.
Ramp, S.R., Rosenfeld, L.K., Tisch, T.D., Hicks, M.R., 1997b. Moored observations of the current and temperature structure over the continental slope off central California. 1. A basic description of the variability. Journal of Geophysical Research 102, 22877–22902.
Rischmiller, F.W., 1993. Variability of the California Current System off Point Sur, California, from April 1988 to December 1990. M.S. Thesis. Naval Postgraduate School, Monterey, 157.
Robinson, A.R., Carton, J.A., Mooers, C.N.K., Walstad, L.J., Carter, E.F., Rienecker, M.M., Smith, J.A., Leslie, W.G., 1984. A real-time dynamical forecast of ocean synoptic/mesoscale eddies. Nature 309 (5971), 781–783.
Robinson, A.R., Carton, J.A., Pinardi, N., Mooers, C.N.K., 1986. Dynamical forecasting and dynamical interpolation: an experiment in the California current. Journal of Physical Oceanography 16, 1561–1579.
Robinson, A.R., Gangopadhyay, A., 1997. Circulation and dynamics of the Western North Atlantic. II. Dynamics of meanders and rings. Journal of Atmospheric and Oceanic Technology 14 (6), 1333–1351.
Robinson, A.R., Glenn, S.M., 1999. Adaptive sampling for ocean forecasting. Naval Research Reviews 51 (2), 28–38.
Robinson, A.R., Glenn, S.M., Spall, M.A., Walstad, L.J., Gardner, G.M., Leslie, W.G., 1989. Forecasting meanders and rings, EOS. Oceanography Report 70 (45), 1464–1473.
Rosenfeld, L.K., Schwing, F.B., Garfield, N., Tracy, D.E., 1994. Bifurcated flow from an upwelling center: a cold source for Monterey Bay. Continental Shelf Research 14, 931–964.
Schmidt, A.C.K., Brickley, P., Gangopadhyay, A., Cadwallader, M., Sharma, N., Nobre, C., Coholan, P., Feeney, J., 2011. A feature oriented regional modeling system for the north Brazil current rings migration after retroflection. In: Proceedings of the Offshore Technology Conference , Houston, Texas, USA, May 2011.
Schmidt, A.C.K., Gangopadhyay, A., under review. An operational ocean circulation prediction system for the northwest Atlantic: validation during July–September of 2006. Continental Shelf Research.
Schofield, O., Glenn, S.M., Orcutt, J., Arrott, M., Meisinger, M., Gangopadhyay, A., Brown, W., Signell, R., Moline, M., Chao, Y., Chien, S., Thompson, D., Balasuriya, A., Lermusiaux, P., Oliver, M., 2010. Automated Sensor Networks to Advance Ocean Science, EOS 91 (September (39)), 2010.
Shaji, C., Gangopadhyay, A., 2007. Synoptic modeling of the West India Coastal Current System using an upwelling feature model. Journal of Atmospheric and Oceanic Technology 24 (5), 877–893.
Sheres, D., Kenyon, K.E., 1989. A double vortex along the California Coast. Journal of Geophysical Research 94, 4989–4997.
Shulman, I., Kindle, J., Martin, P., deRada, S., Doyle, J., Penta, B., Anderson, S., Chavez, F., Paduan, J., Ramp, S., 2007. Modeling of upwelling/relaxation events with the Navy Coastal Ocean Model. Journal of Geophysical Research 112, C06023, doi:10.1029/2006JC003946.
Shulman, I., Rowley, C., Anderson, S., DeRada, S., Kindle, J., Martin, P., Doyle, J., Cummings, J., Ramp, S., Chavez, F.P., Fratantoni, D., Davis, R., 2009. Impact of glider data assimilation on the Monterey Bay model. Deep-Sea Research II, doi:10.1016/j.dsr2.2008.08.003.
Smith, R.C., Dustan, P., Au, D., Baker, K.S., Dunlap, E.A., 1986. Distribution of cetaceans and sea-surface chlorophyll concentrations in the California Current. Marine Biology 91 (3), 385–402, doi:10.1007/BF00428633.
Smith, S.L., Lane, P.V.Z., 1991. The jet off Point Arena, California: its role in aspects of secondary production in the copepod Eucalanus californicus Johnson. Journal of Geophysical Research 96, 14849–14858.
Strub, P.T., James, C., 2000. Altimeter-derived variability of surface velocities in the California Current System. 2. Seasonal circulation and eddy statistics. Deep-Sea Research II 45, 831–870.
Strub, P.T., Kosro, P.M., Huyer, A., 1991. The nature of the cold filaments in the California Current System. Journal of Geophysical Research 96, 14743–14768.
Swenson, M.S., Niiler, P.P., 1996. Statistical analysis of the surface circulation of the California Current. Journal of Geophysical Research 101, 22631–22645.
Tisch, T.D., Ramp, S.R., Collins, C.A., 1992. Observations of the geostrophic current and water mass characteristics off Point Sur, California, from May 1988 through November 1989. Journal of Geophysical Research 97, 12535–12555.
Tracy, D., 1990. Source of cold water in Monterey Bay observed by AVHRR satellite imagery. MS thesis. Naval Postgraduate School, Monterey, CA.
Traganza, E.D., Nestor, D.A., McDonald, A.K., 1980. Satellite observations of a nutrient upwelling off the coast of California. Journal of Geophysical Research 85 (4), 101–106.
Traganza, E.D., Conrad, J.C., Breaker, L.C., 1981. Satellite observations of a cyclonic upwelling system and giant plume in the California Current. In: Richards, F.A. (Ed.), Coastal Upwelling. American Geophysical Union, Washington, DC, pp. 229–241.

Veneziani, M., Edwards, C.A., Doyle, J.D., Foley, D., 2009a. A central California coastal ocean modeling study: 1. Forward model and the influence of realistic versus climatological forcing. Journal of Geophysical Research 114, C04015, doi:10.1029/2008JC004774.
Veneziani, M., Edwards, C.A., Moore, A.M., 2009b. A central California coastal ocean modeling study: 2. Adjoint sensitivities to local and remote forcing mechanisms. Journal of Geophysical Research 114, C04020, doi:10.1029/2008JC004775.
Walstad, L.J., Allen, J.S., Kosro, P.M., Huyer, A., 1991. Dynamics of the Coastal Transition Zone through data assimilation studies. Journal of Geophysical Research 96, 14959–14978.
Warn-Varnas, A., Gangopadhyay, A., Hawkins, J., 2007. Water Masses in the Monterey Bay during summer of 2000. Continental Shelf Research, doi:10.1016/j.csr. 2007.01.004.
Washburn, L., Kadco, D.C., Jones, B.H., Hayward, T., Kosro, P.M., Stanton, T.P., Ramp, S., Cowles, T., 1991. Water mass subduction and the transport of phytoplankton in a coastal upwelling system. Journal of Geophysical Research 96, 14927–14945.
Wickham, J.B., 1975. Observations of the California countercurrent. Journal of Marine Research 33, 325–340.
Wickham, J.B., Bird, A.A., Mooers, C.N.K., 1987. Mean and variable flow over the central California continental margin. Continental Shelf Research 7, 827–849.
Wooster, W.S., Jones, J.H., 1970. California Undercurrent off Northern Baja California. Journal of Marine Research 28, 235–250.
Wyllie, J.G., 1966. Geostrophic flow of the California Current at the surface and at 200 meters. In: California Cooperative Oceanic Fisheries Investigation (CalCOFI), Atlas No. 4, 288 pp.